

Extension of the Karplus Relationship for NMR Spin-Spin Coupling Constants to Nonplanar Ring Systems: Pseudorotation of Tetrahydrofuran

Anan Wu and Dieter Cremer*

Department of Theoretical Chemistry, Göteborg University, S-413 20 Göteborg, Sweden
Tel: +49 (031) 773 5597, Fax +49 (031) 773 5590, E-mail: cremer@theoc.gu.se

Received: 14 September 2002 / Accepted: 10 December 2002 / Published: 4 April 2003

Abstract: Karplus relationships for all 26 NMR spin-spin coupling constants (SSCCs) J of the pseudorotating tetrahydrofuran (THF) molecule were derived by expanding J as a function $J(q, \phi)$ of the puckering amplitude q and the pseudorotational phase angle ϕ . For this purpose, the conformational potential $V(q, \phi)$ of THF was determined at the MBPT(2)/cc-pVTZ and B3LYP/6-31G(d,p) levels of theory. THF is a slightly hindered pseudorotor (MP2 barriers ΔE and ΔH are 0.1 - 0.2 kcal/mol) with a puckering amplitude $q = 0.396 \text{ \AA}$ and a barrier to inversion $\Delta H = 4.1 \text{ kcal/mol}$ in reasonable agreement with experimental data. The SSCCs of THF were calculated both at MBPT(2)/cc-pVTZ and B3LYP/6-31G(d,p) geometries using coupled perturbed density functional theory (CPDFT) with the B3LYP functional and a (9s,5p,1d/5s,1p)[6s,4p,1d/3s,1p] basis set. All geometrical parameters and the 26 SSCCs of THF were computed as functions of the phase angle ϕ and averaged to give $\langle {}^nJ \rangle$ values that can be compared with measured data. The following SSCCs were obtained: $\langle {}^1J(\text{CC}) \rangle = 34.2, 34.0$; $\langle {}^1J(\text{CO}) \rangle = 26.4$; $\langle {}^1J(\text{CH}) \rangle = 142.6, 130.9$; $\langle {}^2J(\text{CXC}) \rangle = 0.5, 0.8$; $\langle {}^2J(\text{OCC}) \rangle = 0.3$; $\langle {}^2J(\text{CCH}) \rangle = -1.5, -0.7, -2.8$; $\langle {}^2J(\text{OCH}) \rangle = -8.6$; $\langle {}^2J(\text{HCH}) \rangle = -8.7, -12.0$; $\langle {}^3J(\text{CXCH}) \rangle = 3.0, 4.0, 2.9$; $\langle {}^3J(\text{OCCH}) \rangle = -1.2$; $\langle {}^3J(\text{HCCH, cis}) \rangle = 7.3, 8.5$; $\langle {}^3J(\text{HCCH, trans}) \rangle = 5.3, 5.5$; $\langle {}^4J(\text{HCXCH, cis}) \rangle = -0.2, -0.2$; $\langle {}^4J(\text{HCXCH, trans}) \rangle = -0.5, -0.6 \text{ Hz}$ ($X = \text{C or O}$). Magnitude and trends in calculated SSCCs are dominated by the Fermi contact term although other contributions are not negligible. Those SSCCs that strongly depend on the pseudorotational mode of THF were identified as suitable descriptors for the conformation of THF in solution. THF is discussed as a suitable model for ribose.

Keywords: NMR spin-spin coupling constants, Karplus relationship, ring puckering, tetrahydrofuran, ribose

1 Introduction

Indirect nuclear magnetic resonance (NMR) spin-spin coupling constants (SSCCs) ${}^nJ(A,B)$ are sensitive to the geometrical features of a molecule and, therefore, their magnitude provides a direct insight into the geometry and electronic structure of a molecule [1-5]. Most celebrated in this connection is the Karplus relationship, which relates in a simple trigonometric way vicinal SSCCs of the type ${}^3J(\text{HCCH})$ to the dihedral angle $\tau(\text{HCCH})$ [6-8]. The Karplus relationship (often called Karplus equation) has been extended beyond the field of proton-proton coupling constants and is extensively used to determine dihedral angles and by this conformational features of molecules, in particular biomolecules, from measured SSCCs [9-11].

In previous work, we described a generalization of the Karplus relationship in the case of pseudorotating ring molecules [12]. In the case of a free (or nearly free) pseudorotor, it is difficult to establish a Karplus relationship because only average SSCCs $\langle J \rangle$ can be measured, which do not seem to provide any insight into conformational features of a molecule. In this situation, however, reliable quantum chemical calculations of individual constants J [13,14] in dependence of the pseudorotational mode of a ring can be used to compliment the limited information obtained from NMR experiments to derive a Karplus relationship for the ring molecule [12]. Our investigation of cyclopentane led to a number of interesting conclusions concerning the description of pseudorotating molecules with the help of SSCCs [12].

- 1) The establishment of a Karplus relationship using the dihedral angles of the ring is problematic because often one dihedral angle can be associated with two different SSCCs. However, a useful extension of the Karplus relationship to pseudorotating rings is achieved by expressing SSCC as a function of the puckering coordinates of the ring molecule.
- 2) For cyclopentane, SSCCs were calculated employing both CCSD theory [15-17] and coupled perturbed DFT (CPDFT) [13] with the B3LYP functional. Both approaches led to reasonable SSCCs. However, for a given basis set of moderate size CPDFT turned out to be superior in terms of both cost and accuracy [12].
- 3) All SSCCs of cyclopentane could be expressed as simple analytical functions of the ring puckering coordinates of a five-membered ring, namely the pseudorotational phase angle ϕ and the puckering amplitude q . Average values $\langle J \rangle$ were calculated by integrating functions $J(\phi)$ over ϕ . Results were compared with measured $\langle J \rangle$ values.
- 4) It was shown that by a combination of measured and calculated $\langle J \rangle$ values, important conformational properties of a ring molecule can be determined.

The work carried out for cyclopentane represents a first step of determining J -hypersurfaces spanned in terms of the most important conformational coordinates of a ring compound. Once a J -hypersurface is known, it can be used to investigate the conformational behavior of biochemically

interesting molecules such as ribose, 2'-deoxyribose, proline, etc.

In this work, we extend the investigation of pseudorotating ring molecules to tetrahydrofuran (THF). THF is the appropriate test case in connection with an NMR-spectroscopic investigation of ribose. Hence, we will determine the the pseudorotational potential of THF, then calculate all NMR SSCCs of THF for selected molecular forms located along its pseudorotational path. These SSCCs will be the basis to derive Karplus relationships of the form $J = J(q, \phi)$, which reflects the conformational behavior of THF.

Because of its importance as a model for ribofuranose, THF has been extensively investigated by various experimental techniques ranging from far-infrared spectroscopy [18,19] and microwave spectroscopy [20,21] to electron diffraction [22], X-ray [23], and neutron diffraction techniques [24]. In addition, there are several quantum chemical investigations [25,26] and molecular mechanics (MM) studies [27,28], which have focused on the conformational features of THF. However, relative little is known about the SSCCs of THF either from experiment [29,30] or theory [31-33] so that the current investigation fills a gap in the description of this important molecule.

2 Computational Methods

In the following, the theory of ring puckering coordinates, the quantum chemical methods used, and the derivation of the Karplus relationships used in this work are shortly described.

Description of THF in terms of Ring Puckering Coordinates. As shown by Cremer and Pople (CP) [34], the conformational space of any puckered N-membered ring can be spanned by N-3 puckering coordinates, which split up in pairs of pseudorotational coordinates q and ϕ , and (for even-membered rings) an additional puckering amplitude describing ring inversion. Hence, for THF ($N = 5$) there is just one pseudorotational mode defined by the pseudorotational phase angle ϕ describing the mode of ring puckering and the puckering amplitude q describing the degree of ring puckering [25,34]. An infinite number of ring conformations is located along the pseudorotational path, of which in the case of THF a subset of 20 forms is easy to recognize because it comprises the ten envelope (E) forms ($\phi = (0 + k*360)/10$ for $k = 0,1,2,\dots,9$) and the ten twist (T) forms ($\phi = (18 + k*360)/10$ for $k = 0,1,2,\dots,9$) of a five-membered ring (see Figure 1). Since planar THF possesses C_{2v} symmetry, the conformational energy surface (CES) must comply with this symmetry, which means that puckered THF forms with $\phi = 0 \pm \Delta\psi$ and $\phi = 180 \pm \Delta\psi$ are identical for unsubstituted THF (see Figure 1). There are just three unique E ($\phi = 0, 36, 72^\circ$), three unique T forms ($\phi = 18, 54, 90^\circ$), and the planar form ($q = 0, \phi$ not specified), which have to be considered in an investigation of THF. Of course, this minimum set of conformations can be augmented, if necessary, by setting the phase angle to other values than those of the T and E forms.

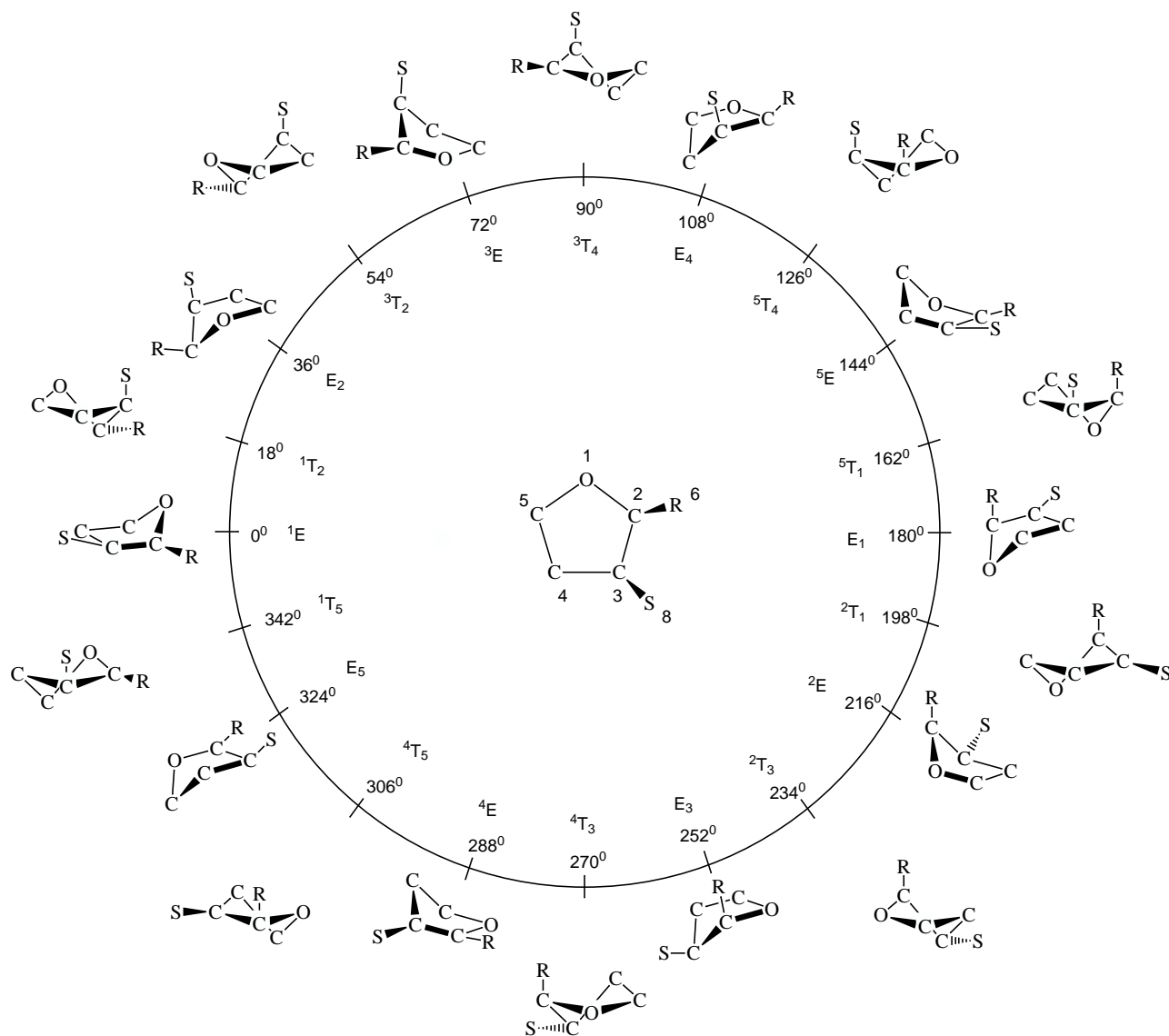


Figure 1: Pseudorotation itinerary ($\phi = 0 \rightarrow 360^\circ$) of tetrahydrofuran (THF) as indicated by the 10 E and ten T forms at $\phi = (0 + k \cdot 360) / 10$ and $\phi = (18 + k \cdot 360) / 10$ ($k = 0, 1, 2, \dots, 9$). At the center ($q = 0$), the planar ring is located. To distinguish different positions in the ring, symbols R, S are used for substituents.

According to the CP theory of ring puckering, the out-of-plane coordinates z_j of atom $j=1,\dots,5$ of any five-membered ring conformation are given by [34-41]

$$z_j = \left(\frac{2}{5}\right)^{1/2} q \cos\left[\frac{4\pi(j-1)}{5} + \phi\right] \quad \text{for } j = 1, \dots, 5 \text{ and } \phi[0; 2\pi] \quad (1)$$

where the coordinates z_j are normalized according to

$$\sum_{j=1}^5 z_j^2 = q^2 \quad (2)$$

The full set of $3N-6$ independent Cartesian coordinates of any puckered N -membered ring can be determined once the $N-3$ puckering coordinates ($N = 5$: q and ϕ), $N-3$ bond angles ($N = 5$: two internal ring angles of the five-membered ring), and N (5) bond lengths are specified. First, the z_j coordinates are calculated according to Eq. (1) (or similar formulas for $N > 5$) [34,35]; then the N bond lengths and $N-3$ bond angles are projected onto the mean plane of the ring. Finally, the projected ring is partitioned into segments, for which the coordinates x_j, y_j are calculated according to a procedure described by Cremer [37].

The use of the ring puckering coordinates has the advantage [40,41] that the geometry of puckered forms of THF with a given value of ϕ (or q and ϕ) can be optimized even if these forms do not occupy a stationary point of the CES. This would not be possible when using Cartesian or internal coordinates [37]. Another advantage results from the fact that any calculated property of THF (in particular any SSCC) can be expressed as a function of the puckering coordinates.

In Figure 1, the planar form, ten E and ten T forms of THF are shown in the conformational space spanned by q and ϕ . Hence, the planar form is located at the center for $q = 0$ and the puckered E and T forms along a pseudorotation itinerary (given by a circle). The numbering of the ring atoms (see Figure 1) defines the conformation at $\phi = 0^\circ$ and all subsequent conformations. Often the different E and T forms are identified according to a notation based on suitable reference planes taken from the E (atoms 2, 3, 4, 5) and the T form (atoms 1, 2, 5) of cyclopentane. Ring atoms, which lie above the reference plane are written as superscripts and precede the conformational symbol E or T, while ring atoms, which lie below the reference plane are written as subscripts and follow the symbol E and T [42]. Since experimentalists often prefer this notation instead of using puckering coordinates, it is also given in Figure 1. However, in the discussion, we will exclusively use the pseudorotational angle to identify a given ring form since this notation can be applied to any ring form in the pseudorotational space.

Quantum Chemical Methods and Basis Sets. Energies, geometries, frequencies, enthalpies, and density distributions of seven THF forms were calculated by using second-order many-body perturbation theory [MBPT(2)] with the Møller-Plesset (MP) perturbation operator [43] and

Dunning's cc-pVTZ basis set [44]. This level of theory leads to a very accurate description in the case of cyclopentane as we showed recently [12]. Since the actual target of the current project is the investigation of larger ring systems such as ribose and 2'-deoxyribose sugars, for which MBPT(2)/cc-pVTZ calculations become too expensive in view of the large number of conformations involved, the usefulness of a more economic method was also tested in this work. For this purpose, a second set of calculations was carried out using density functional theory (DFT) [45,46] with the hybrid functional B3LYP [47-49] and Pople's 6-31G(d,p) basis set [50]. For the B3LYP frequency calculations, an ultrafine pruned (99,590) grid was used.

Geometries were calculated with the help of analytical gradients for ring puckering coordinates developed by Cremer [37]. These were also used to calculate vibrational frequencies and to determine zero-point energies (ZPE) and enthalpies H(298) at 298 K. When calculating the vibrational contributions to enthalpies, large amplitude vibrations corresponding to the ring puckering modes were treated separately similar to the way internal rotations are treated [51].

The electron density distribution, atomic charges, and the degree of hybridization was investigated by calculating MP2 response densities [52,53] and applying Weinhold's natural bond orbital (NBO) analysis [54-56].

Calculation of the CES of THF. The CES function $V(q, \phi)$ of any puckered five-membered ring can be given as a Fourier expansion in the pseudorotational phase angle ϕ and a power series in the puckering amplitude q [25,12]:

$$V(q, \phi) = \sum_{k=0}^{\infty} \{V_k^c(q) \cos(k\phi) + V_k^s(q) \sin(k\phi)\} \quad (3)$$

where V_k^c and V_k^s are expressed as

$$V_k(q) = \sum_{l=0}^{\infty} V_{kl} q^l \quad (4)$$

In view of the C_{2v} -symmetry of planar THF, the CES function $V(q, \phi)$ can be simplified and truncated after the quartic term according to Eq. (5):

$$V(q, \phi) = V_{00} + V_{02} q^2 + V_{04} q^4 + V_{22} q^2 \cos(2\phi) + V_{24} q^4 \cos(2\phi) + V_{42} q^2 \cos(4\phi) + V_{44} q^4 \cos(4\phi) \quad (5)$$

where the constant V_{00} is set equal to the energy of the planar ring. Coefficients V_{02}, \dots, V_{44} were determined by optimizing the geometry of the six puckered ring forms with $\phi = 0, 18, 36, 54, 72,$ and 90° .

Similarly to V , each property P of THF can be expressed as a function of the puckering coordinates. Global properties P of the molecule lead to functions $P(\phi)$, which always comply with the molecular symmetry whereas local properties can lead Fourier expansions in ϕ of lower symmetry.

In the latter case, the property in question has to be determined for all 20 THF forms given in Figure 1 (and others not considered there) to obtain accurate functions $P(\phi)$. Nevertheless, the symmetry of the molecule helps again to reduce the number of necessary calculations. For example, calculation of the E form at $\phi = 0$ leads to the length of the equatorial bond C2H6, but provides also the length of this bond at $\phi = 180$ where it occupies an axial position and becomes identical to the length of the axial bond C2H7 at $\phi = 0$. Use of Figure 1 helps to identify these relationships.

Calculation of the SSCCs of THF. SSCCs were determined by coupled perturbed density functional theory (CPDFT) as recently described and implemented by Cremer and co-workers [13]. In this approach, Fermi contact (FC), paramagnetic spin-orbital (PSO), diamagnetic spin-orbit (DSO), and spin-dipole (SP) contribution to the total SSCC are consistently determined at the CPDFT level of theory (see also Ref. 57). Previous investigations showed that reliable SSCC values are obtained with the B3LYP functional [12,13,57] and TZ+P or QZ+P basis sets [58]. In this work, a (9s,5p,1d/5s,1p)[6s,4p,1d/3s,1p] basis set was employed (basis II of ref 58).

Using CPDFT/B3LYP all SSCCs of the type $J(^{13}\text{C}, ^{13}\text{C})$, $J(^{17}\text{O}, ^{13}\text{C})$, $J(^{13}\text{C}, ^1\text{H})$, $J(^{17}\text{O}, ^1\text{H})$ and $J(^1\text{H}, ^1\text{H})$ were calculated. In the following, we will simplify the notation of SSCCs by using symbols such as $^3J(\text{HCCH}, \text{cis})$ where C and H denote ^{13}C and ^1H , the major coupling path H-C-C-H of the 3-bond SSCC is given, and *cis* identifies the positions of the H atoms on the same side of the ring.

SSCCs were calculate for both MBPT(2) and B3LYP geometries. However, because the current work will provide reference data for a B3LYP investigation of ribofuranose, for which MBPT(2)/cc-pVTZ geometry optimizations become too expensive, we will exclusively discuss the SSCCs calculated for the B3LYP/6-31G(d,p) geometries of THF.

For the analysis of the FC term, the *s*-density at the nucleus *K* was calculated according to

$$\varrho_s(K) = \langle \phi_l | \delta(\mathbf{r}_K) | \phi_l \rangle \quad (6)$$

where $\delta(\mathbf{r}_K)$ is the Dirac delta function and ϕ_l is the localized bond orbital. The product $\varrho_s(K, L) = \varrho_s(K)\varrho_s(L)$ was related to the magnitude of the FC term.

Calculation of the Karplus Relationships $J(q, \phi)$ or $J(\phi)$. The SSCC nJ was expanded as a function of the puckering coordinates *q* and ϕ according to Eq. (7).

$$^nJ(q, \phi) = A_0(q) + \sum_{k=1}^{\infty} B_k(q) \cos(k\phi) + C_k(q) \sin(k\phi) \quad (7)$$

where the term $A_0(q)$ converges to the SSCC of the planar ring for $q \rightarrow 0$. A_0 , B_k and C_k can be expanded as power series in the puckering amplitude *q*.

$$A_0(q) = \sum_{l=0}^{\infty} A_{0l}q^l \quad (8a)$$

$$B_k(q) = \sum_{l=1}^{\infty} B_{kl}q^l \quad (8b)$$

$$C_k(q) = \sum_{l=1}^{\infty} C_{kl}q^l \quad (8c)$$

Note that for B_k and C_k the constant terms with $l = 0$ vanish because

$$\lim_{q \rightarrow 0} B_k(q) = 0 \quad \text{and} \quad \lim_{q \rightarrow 0} C_k(q) = 0.$$

For pseudorotating ring molecules, only average SSCCs can be measured. For the purpose of calculating average SSCCs, one has to determine both the CES function V and the SSCCs as a function of puckering coordinates q and ϕ . Averaging of the SSCC can be simplified by considering just the dependence of nJ on the pseudorotational phase angle ϕ :

$${}^nJ(\phi) = A_0 + \sum_{i=1}^c B_i \cos(i\phi) + \sum_{j=1}^s C_j \sin(j\phi) \quad (9)$$

where c and s are truncation limits, which can differ. Then, the average SSCC $\langle {}^nJ \rangle$ is given by

$$\langle {}^nJ \rangle = \int_0^{2\pi} \varrho(\phi) {}^nJ(\phi) d\phi \quad (10)$$

The conformational probability distribution $\varrho(\phi)$ is given as a Boltzmann distribution:

$$\varrho(\phi) = \frac{e^{-[V(\phi)-V(0)]/RT}}{\int_0^{2\pi} e^{-[V(\phi)-V(0)]/RT} d\phi} \quad (11)$$

The potential V is determined according to Eq. (5) and used to calculate average SSCCs according to Eq.s (10) and (11).

For the quantum chemical calculations, the program systems COLOGNE2002 [59] and Gaussian98 [60] were used.

3 The Flexible Pseudorotor THF

Calculated energies and puckering coordinates obtained in this work are summarized in Table 1. A three-dimensional perspective drawing of the calculated CES $V(q, \phi)$ is given in Figure 2. The geometries of the planar form, the E form with $\phi = 0^\circ$, and the T form $\phi = 90^\circ$ are shown in Figure 3.

The gross features of the CES of THF resemble those of the CES of cyclopentane (see Figure 2). Incorporation of a hetero atom into the ring makes THF a slightly hindered pseudorotor (energy barrier 0.14 kcal/mol, Table 1). Both MBPT(2) and B3LYP predict a twofold pseudorotational

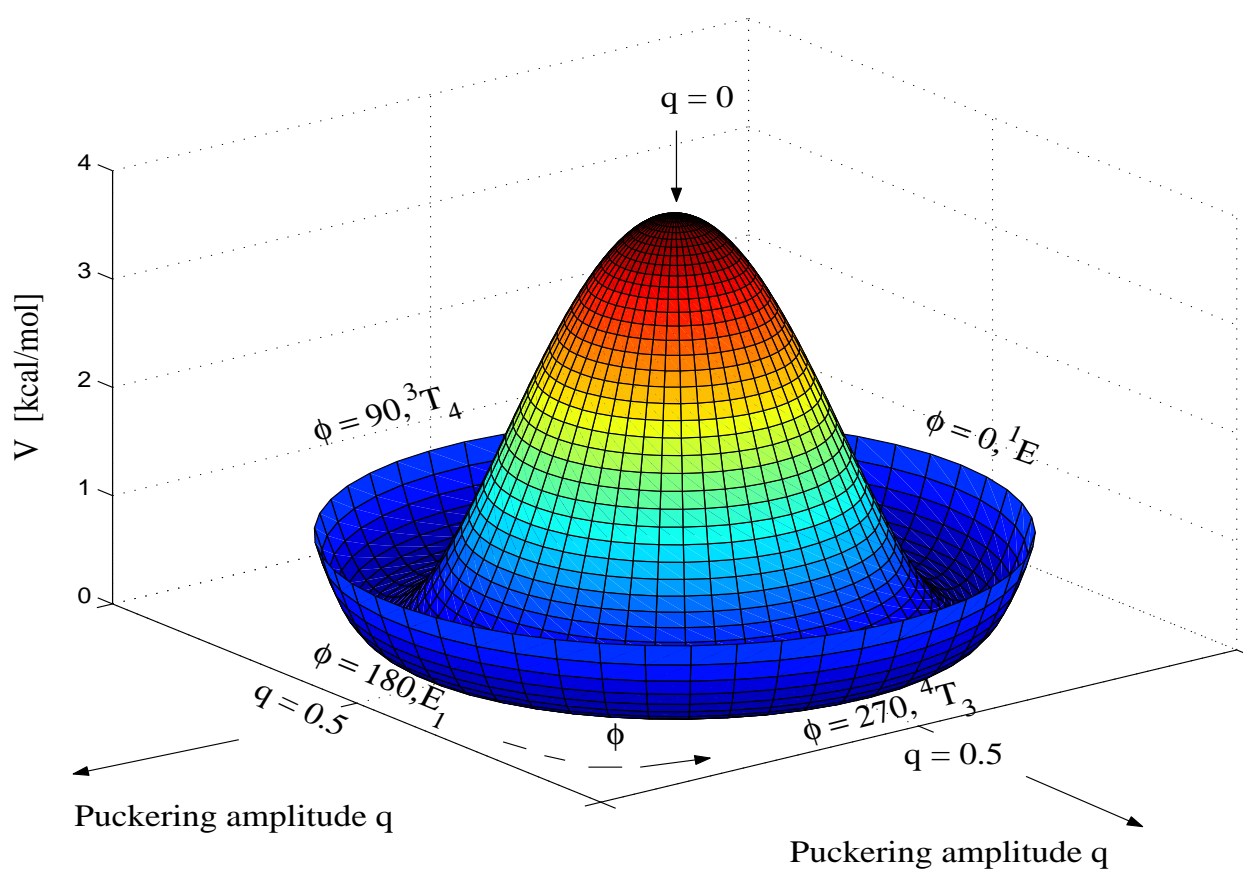


Figure 2: Perspective drawing of the three-dimensional conformational energy surface $V(q, \phi)$ of THF. The planar form with $q = 0$ is located at the maximum. The direction of radial coordinate q and the angular coordinate ϕ is indicated.

Figure 3

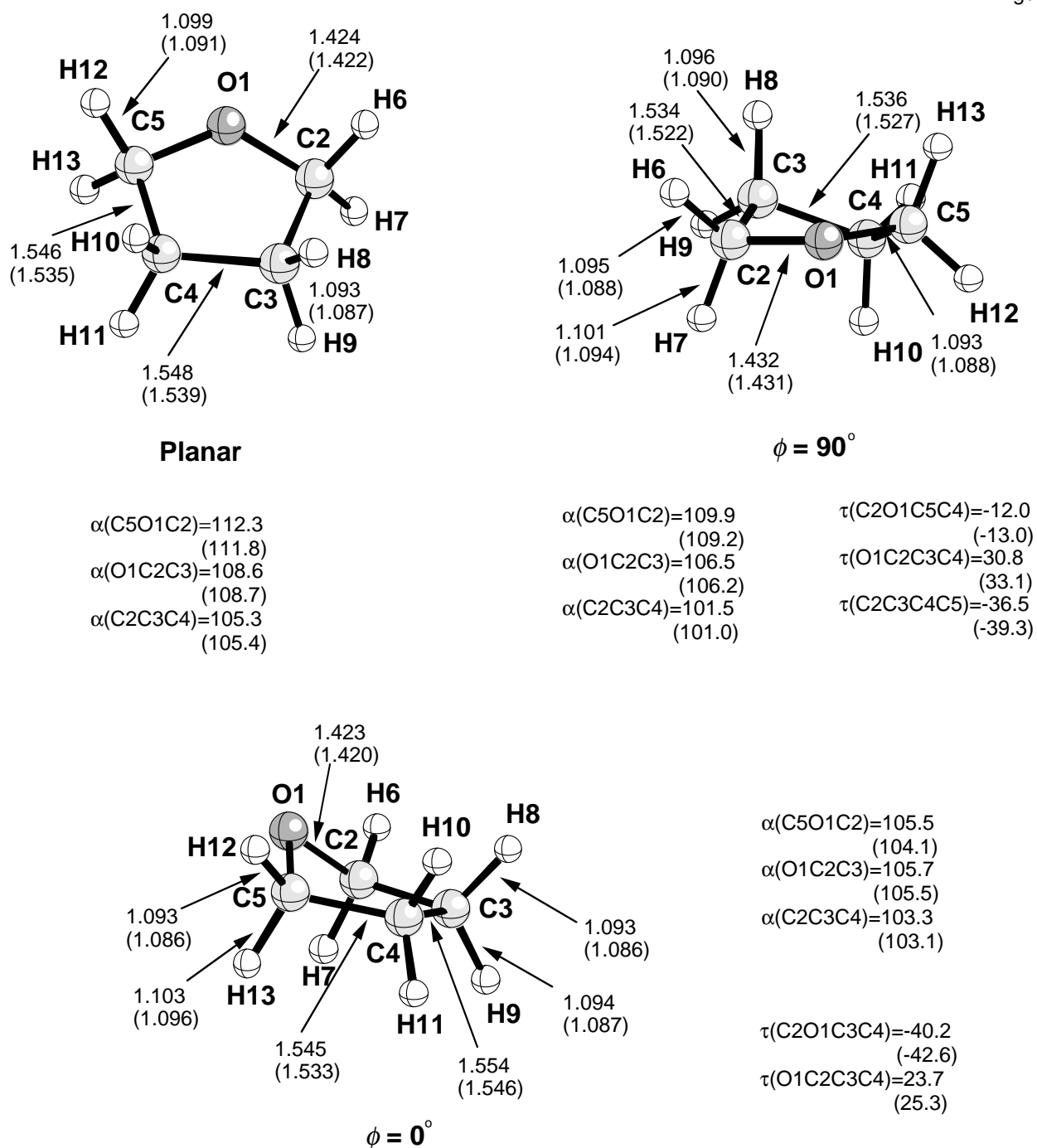


Figure 3: B3LYP/6-31G(d,p) geometries and MBPT(2)/cc-pVTZ geometries (in parentheses) of planar and two puckered ($\phi = 0$ and 90°) THF forms.

potential that locates the T forms with C_2 -symmetry ($\phi = 90^\circ, 270^\circ$) at the the global minima of the CES. The E forms at $\phi = 0^\circ$ and 180° represent first order saddle points of the pseudorotational mode while the planar form occupies a local maximum at the center of the q, ϕ -coordinate system (Figure 2). This is consistent with all previous *ab initio* and MM calculations [25-28] and with

Table 1. Calculated puckering coordinates, energies, and enthalpies of THF. ^a

Method/basis	ϕ	Symbol	Sym	q	ΔE^b	$\Delta H(298)^b$
B3LYP/6-31G(d,p)						
		Planar	C_{2v}	0.000	3.36	2.94
	0	1E	C_s	0.372	0.14	0.25
	18	1T_2	C_1	0.371	0.13	0.23
	36	E_2	C_1	0.371	0.12	0.19
	54	3T_2	C_1	0.371	0.08	0.12
	72	3E	C_1	0.370	0.03	0.03
	90	3T_4	C_2	0.371	0.00	0.00
MBPT(2)/cc-pVTZ						
		Planar	C_{2v}	0.000	4.46	4.15
	0	1E	C_s	0.396	0.14	0.22
	18	1T_2	C_1	0.398	0.11	0.21
	36	E_2	C_1	0.398	0.11	0.20
	54	3T_2	C_1	0.394	0.10	0.17
	72	3E	C_1	0.395	0.04	0.07
	90	3T_4	C_2	0.396	0.00	0.00
exp				0.38 ^c		-3.49(-3.86) ^d

a) Puckering amplitudes q in Å, absolute energies (enthalpies) in hartree, and relative energies (enthalpies) in kcal/mol. For the definition of THF forms, see Figure 1. - b) Energies of the planar form are -232.454942 hartree at B3LYP, -231.972593 at MBPT(2). The corresponding enthalpies are -232.333748 and -231.850089 hartree, respectively. - c) Ref. 22. d) Ref.s 19,20.

most, but not all experimental studies. An electron diffraction study of Bartell and co-workers [22] also predicts the C_2 -symmetrical T forms to represent the equilibrium conformation of THF.

Results based on far-infrared spectroscopy [18,19] are in linewith this. However, microwave studies by Engerholm and co-workers [20] carried out in the late 60ies and recently repeated and extended by Meyer and co-workers [21] suggest a fourfold pseudorotational potential (V_{4l} coefficients dominate the CES function (5) rather than the V_{2l} coefficients) with equivalent minima at $\phi = 0 \pm 52.5^\circ$ and $180 \pm 52.5^\circ$, which are close to the T forms at $\phi = 54, 126, 234,$ and 306° .

A careful analysis of calculated energies and geometries (see below) provides now clue for a fourfold pseudorotational potential. In particular, the analysis of the electronic effects determining the stability of the various THF forms along the pseudorotation path clearly suggests the T forms at $\phi = 90$ and 270° to be more stable than any other T form. The argument given by Meyer and co-workers [21] that *ab initio* theory is not sufficiently accurate to provide a reliable description of the pseudorotational potential of THF has to be rejected on the following grounds. The quantum chemical description of conformational processes does not require high-level correlation corrected *ab initio* methods because the bonding pattern of the molecule (and by this also the pair correlation effects) remains largely unchanged during internal rotation, pseudorotation, etc. Although MBPT(2) covers just pair correlation effects [43], it is known to provide an accurate account of energies and geometries along the pseudorotational path of a free (or slightly hindered) pseudorotor if carried out with a cc-pVTZ basis set [12,35]. The consistency of the MBPT(2) description along the pseudorotation itinerary excludes the existence of C_1 -symmetrical minima as suggested by the microwave results.

It is noteworthy in this connection that both the spectroscopic [18-21] and the electron diffraction study [22] had to fit experimental parameters such as diffraction intensities, frequency splittings (due to tunneling) or rotational constants to a constrained model of THF based on assumed geometrical parameters and simplifications of its conformational flexibility. A more direct way of determining the equilibrium conformation of THF was provided by X-ray diffraction experiments at 103 K of Luger and Buschmann [23] and the high resolution neutron powder diffraction experiments at 5 K of David and Ibberson [24]. Both investigations identify the T forms at $\phi = 90^\circ$ and 270° as the equilibrium forms of THF in line with the twofold pseudorotational potential calculated in this work.

The enthalpy barriers ΔH along the pseudorotational path obtained from MBPT(2) and B3LYP calculations are 0.22 and 0.25 kcal/mol (Table 1), respectively, corresponding to 77 and 87 cm^{-1} , which are in good agreement with experimental estimates from a far-infrared measurement (< 0.5 kcal/mol) [18], and from microwave experiments (0.21 kcal/mol or 73 cm^{-1} [20]; 0.13 kcal/mol or 45 cm^{-1} [21]). The barrier to planarity, $\Delta E(\text{inv})$ ($\Delta H(\text{inv})$), is calculated to be 3.36 (2.94) kcal/mol at B3LYP and 4.46 (4.15) kcal/mol at MBPT(2) (see Table 1). Both $\Delta H(\text{inv})$ values compare well with experimental estimates of 3.49 kcal/mol (microwave spectroscopy [20]) and 3.86 kcal/mol (far-infrared experiment [19]). B3LYP seems to slightly underestimate, MBPT(2) to

Table 2. Fourier expansions for geometrical parameters of THF.^a

Parameter	Definition	A	B ₁ cos ϕ	B ₂ cos 2 ϕ	B ₃ cos 3 ϕ	B ₄ cos 4 ϕ	B ₅ cos 5 ϕ	C ₁ sin ϕ	C ₂ sin 2 ϕ	C ₃ sin 3 ϕ	STD
R(CH)	C2H6	1.0982	-0.0051					-0.0022	0.0006		0.0000 ₃
R(CH)	C3H8	1.0941		-0.0006				0.0010			0.0000 ₂
R(CC)	C3C4	1.5436		0.0090		0.0013					0.0001
R(CC)	C2C3	1.5399		0.0054		-0.0011			0.0107		0.0002
R(OC)	O1C2	1.4275		-0.0044					-0.0041		0.0002
α (OCH)	O1C2H6	109.15	-1.6846	-0.0369	0.4960		-0.03226	-0.2548	0.3083	0.0657	0.02
α (OCC)	O1C2C3	105.98	-0.0019	-0.3703	-0.0019	0.0891	-0.0019		1.2968		0.05
α (COC)	C2O1C5	107.83		-2.2607		-0.0894					0.01
α (CCC)	C2C3C4	102.47		0.8849		-0.0306			-0.8383		0.09
α (CCH)	C2C3H8	111.47	-0.5724	-0.1827	0.0704	-0.0245	-0.0056	-1.5752	0.0060	-0.3957	0.03
α (CCH)	C3C2H6	112.21	1.8331	0.1165	-0.0724	-0.0499	-0.0132	0.8235	0.2527	-0.2525	0.02
α (CCH)	C3C4H10	111.79	-0.6000	-0.1192	-0.4023	0.0471		1.6042	-0.1720	-0.0677	0.01
α (HCH)	H6C2H7	108.09		0.2028		0.0081			0.1818		0.01
α (HCH)	H8C3H9	107.81		-0.2265		-0.0074			0.4099		0.03
τ (OCC H)	O1C2C3H8	-119.74	24.6323	-0.2656	0.4331	-0.0152	0.0066	33.44	0.2589	0.1660	0.05
τ (C CC H)	C2C3C4H10	-119.52	0.9530	-0.2253	0.1433	0.0253	0.0080	-38.9574	-0.3837	-0.3755	0.04
τ (C OC H)	C2O1C5H12	121.04	41.4558	-0.0951	0.0974	-0.0049	-0.0225	-12.9944	0.2854	0.1810	0.03
τ (C CC H)	C4C3C2H6	119.04	22.6255	-0.2121	0.5266	0.0334	-0.035	30.9572	-0.2993	-0.0413	0.05
τ (H CC H)	H6C2C3H8	-0.7008	23.5883	-0.4798	0.9996	0.0158	-0.0300	33.5767	-0.0400	0.0834	0.07
τ (H CC H)	H8C3C4H10							41.5628	-0.7677	-0.8249	0.05
τ (H CC H)	H6C2C3H9	-121.21	23.5895	0.0543	1.0008	0.0489	-0.0290	33.5765	-0.5585	0.0837	0.05
τ (H CC H)	H8C3C4H11	120.96		-0.4512		0.0502		41.5632		0.8250	0.02
τ (C CCC)	C2C3C4C5							-36.352		0.0742	0.04

a) The Fourier expansion given in Eq. (12) was used. Coefficients B_i and C_j associated with $\cos(i\phi)$ and $\sin(j\phi)$, respectively, are listed. The numbering of atoms corresponds to that shown in Figures 1 and 3.

slightly overestimate the barrier to planarity as was also observed in the case of cyclopentane [12].

All E and T forms are predicted to have the same puckering amplitude q (B3LYP: 0.371 ± 0.001 ; MBPT(2), 0.396 ± 0.002 Å; Table 1), which is typical of a free or slightly hindered pseudorotor [12,25]. Agreement with the puckering amplitude $q_g = 0.38 \pm 0.02$ Å obtained in the electron diffraction experiment [22] is satisfactory considering vibrational effects and the fact that the latter investigation used a highly constrained geometrical model (e.g., equal CC and CO bond lengths) of THF. David and Ibberson determined a q value of 0.343 Å for the T forms ($\phi = 90^\circ, 270^\circ$) on the basis of the neutron diffraction data [24] while the X-ray diffraction study of Luger and Buschmann [23] led to a q value of 0.348 Å. Considering again vibrational effects and the fact that the interactions between THF molecules in the unit cell imply a slight flattening of the five-membered ring, agreement with theory is reasonable.

Table 3. Average geometrical parameters of THF calculated at B3LYP/6-31G(d,p) and MBPT(2)/cc-pVTZ. ^a

Parameter	B3LYP Average	MP2 value ^b	ED ^c	B3LYP C_2 form $\phi = 90, 270^\circ$	MP2	X-ray ^d C_2 form	ND ^e C_2 form
O1C2	1.428	1.426	1.428	1.432	1.431	1.429	1.438
C2C3	1.540	1.529	1.536	1.534	1.522	1.511	1.516
C3C4	1.543	1.534	1.536	1.536	1.527	1.511	1.524
C2H6	1.098	1.091	1.115	1.095	1.088	1.050	1.094 ^f
C3H8	1.094	1.088	1.115	1.096	1.090	1.050	1.096 ^f
$\alpha(C2O1C5)$	108.0	106.8	110.5	109.9	109.2	108.2	109.9
$\alpha(O1C2C3)$	106.0	105.8	106.5	106.5	106.2	107.4	106.4
$\alpha(C2C3C4)$	102.4	102.0	101.8	101.5	101.0	102.0	102.6
q (Å)	0.371	0.396	0.38	0.371	0.396	0.348	0.343

a) See Eq. (10) for the calculation of average values. - b) Averaged over the pseudorotational mode. - c) Electron diffraction data, taken from Ref. 22. - d) X-ray diffraction data at -170°C , taken from Ref. 23. - e) Neutron diffraction data at 5K, taken from Ref. 24. - f) Bond length for C-D. average geometrical parameters

Previous computational investigations of THF were carried out with MM methods ($\Delta E = 1.4$ kcal/mol, $q = 0.370 - 0.399$ Å) [27,28], at the Hartree-Fock level of theory ($\Delta E(\text{inv}) = 2.30 -$

3.41 kcal/mol; $q = 0.314 - 0.370 \text{ \AA}$) [25,26], or at the MBPT(2) level of theory ($\Delta E(\text{inv}) = 4.77 \text{ kcal/mol}$; $q = 0.395 - 0.398 \text{ \AA}$) [26]. Calculated pseudorotational barriers ranged from 0.39 to 0.65 kcal/mol [25,26]. None of these investigations provided an accurate account of the CES of THF because either force fields of moderate accuracy, uncorrelated wave functions, too small basis sets, just constrained geometry optimizations, or ΔE rather than ΔH (neglect of vibrational effects) were used because of computational limitations.

Each geometrical parameter P of THF was expanded in this work using the general Eq. (12):

$$P(\phi) = A_0 + \sum_{i=1}^c B_i^P \cos(i\phi) + \sum_{j=1}^s C_j^P \sin(j\phi) \quad (12)$$

In Table 2, the Fourier expansion coefficients B_i^P and C_j^P of the internal coordinates of THF are listed. In view of the low energy barriers to pseudorotation, the constant term A_0^P of the Fourier expansion is close to the average value $\langle P \rangle$ obtained when using Eq. (12) in connection with (10) and considering the correct Boltzmann statistics (11) for the pseudorotational itinerary (compare with Table 3).

In Table 3, calculated average values $\langle P \rangle$ of the the most important geometrical parameters of THF are compared with available experimental values. Comparison of these data reveals that both MBPT(2) and B3LYP provide a reasonable account of the geometry of THF.

For the purpose of rationalizing the relative stability of the various THF forms along the pseudorotation itinerary, we next consider changes in the internal coordinates caused by a variation of ϕ . In Figure 4, $P(\phi)$ is given for some of the internal coordinates of THF (see also Table 2).

The known rotational barriers of ethane (2.9 kcal/mol) [61,62] and methanol (1.1 kcal/mol) [63,64] suggest that bond eclipsing in the $\text{H}_2\text{C}_3\text{C}_4\text{H}_2$ unit for $\phi = 0^\circ$ and 180° causes a destabilization of the two E forms accompanied by a lengthening of the C3C4 bond to 1.554 Å (see, Figure 4a). For the two T forms at $\phi = 90^\circ$ and 270° bond staggering in the $\text{H}_2\text{C}_3\text{C}_4\text{H}_2$ unit is maximized (see Figure 4c) thus yielding a shorter C3C4 bond (1.536 Å) and larger stability of THF. For the $\text{H}_2\text{C}_2\text{C}_3\text{H}_2$ ($\text{H}_2\text{C}_4\text{C}_5\text{H}_2$) unit bond staggering is maximized for $\phi = 54^\circ$ and 234° ($\phi = 128^\circ$ and 306°) (compare with bond length C2C3 in Figure 4a). Any model of THF, which exaggerates this effect by using a too large barrier to rotation in methanol, gets the four C_1 -symmetrical T forms too stable (see above).

In addition to bond eclipsing/bond staggering effects, there are also anomeric interactions [12,65] involving an O electron lone pair and bonds C2H6 and C2C3. In the case of bond C2C3, they enhance changes in its length to $\Delta = 0.024 \text{ \AA}$ (variation from 1.530 Å at $\phi = 54^\circ$ to 1.554 Å at $\phi = 144^\circ$, see, Figure 4a) while for bond C2H6 Δ is about 0.01 Å. At $\phi = 198 (18)^\circ$, bond C2H6 (C2H7) is perfectly positioned to support a delocalization of one of the lone pair electrons at O into its $\sigma^*(\text{CH})$ orbital. This leads to a weakening of the CH bond but a strengthening of the CO

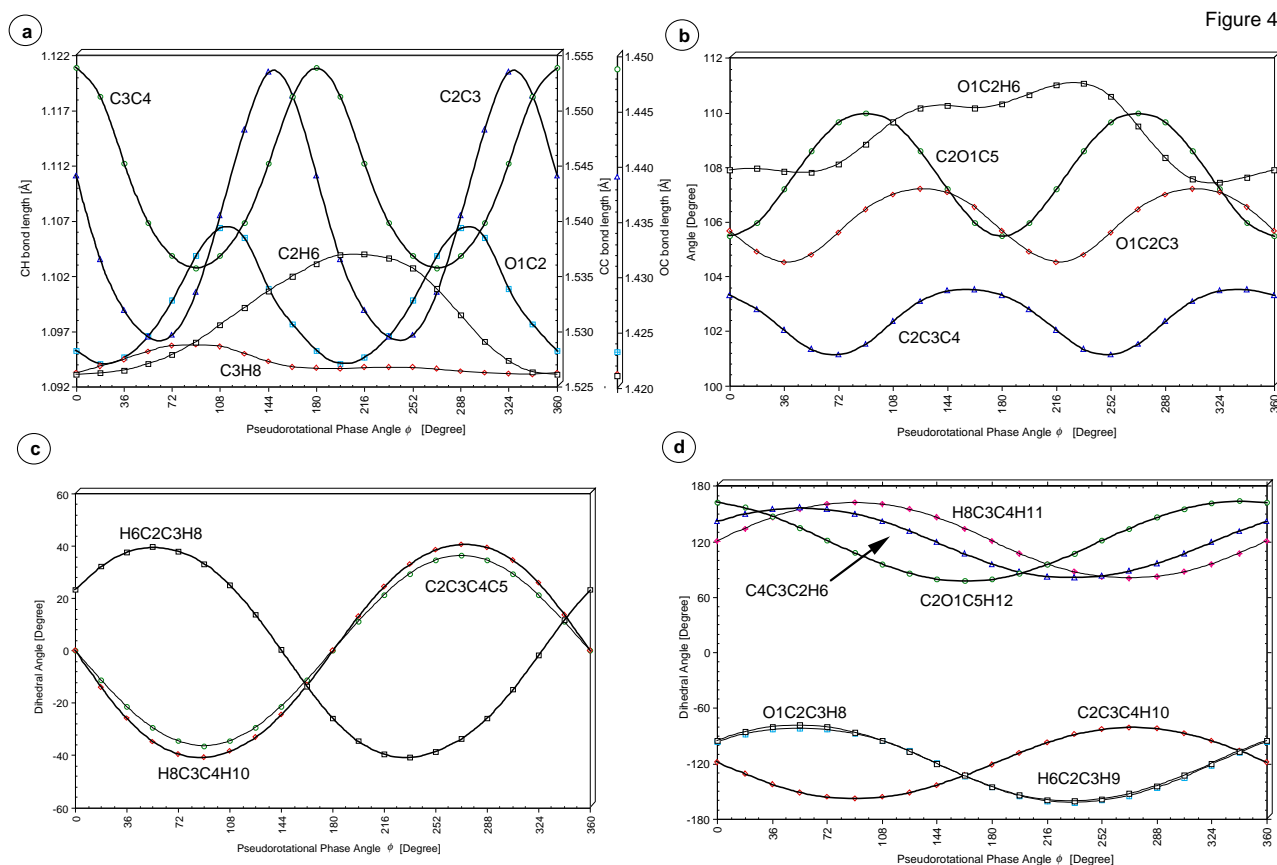


Figure 4: Dependence of the internal coordinates of THF on the pseudorotational phase angle ϕ . (a) Bond lengths $R(O1C2)$, $R(C2C3)$, $R(C3C4)$, $R(C2H6)$ and $R(C3H8)$. (b) Bond angles $\alpha(O1C2C3)$, $\alpha(C2C3C4)$, $\alpha(C2O1C5)$ and $\alpha(O1C2H6)$. (c) Dihedral angles $\tau(C2C3C4C5)$, $\tau(H8C3C4H10)$ and $\tau(H6C2C3H8)$. (d) Dihedral angles $\tau(O1C2C3H8)$, $\tau(C2O1C5H12)$, $\tau(C2C3C4H10)$, $\tau(C4C3C2H6)$, $\tau(H6C2C3H9)$, and $\tau(H8C3C4H11)$. For the numbering of atoms, see Figures 1 and 3. The Fourier expansion coefficients are given for each parameter in Table 2 calculated at B3LYP/6-31G(d,p).

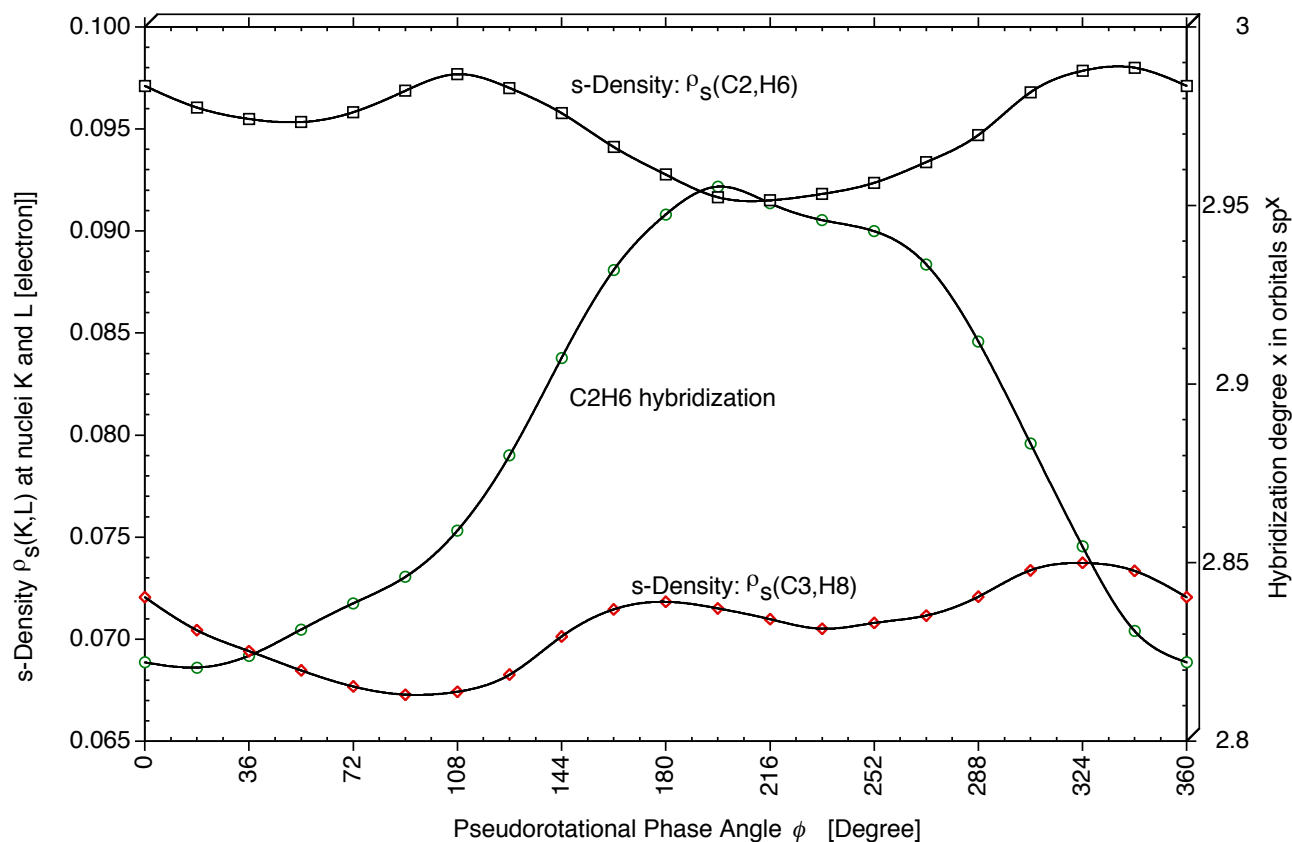


Figure 5: Dependence of the s -densities $\rho_s(K, L) = \rho_s(K)\rho_s(L)$ of CH bonds on the pseudorotational phase angle. The hybridization of the C2H6 bond orbital as calculated with the NBO approach is also given. B3LYP/6-31G(d,p) calculations.

bond (see Figure 4a). The anomeric effect implies that the p -character of the CH bond orbital increases. Hybrid orbital calculations for THF employing the NBO analysis [54-56] confirm this, although effects are small: For C2H6, hybridization changes from $sp^{2.82}$ ($\phi = 18^\circ$) to $sp^{2.96}$ ($\phi = 198^\circ$) (see Figure 5), which corresponds to a slight decrease in the s -character of the CH hybrid orbital from 26.2% to 25.2%. These changes are interesting in view of the changes calculated for the SSCs $^1J(\text{CH})$ (see next section).

The C2O1C5 bond angle changes by 4.5° from 105.5° to 110.0° where the smallest angle is found for the E forms at $\phi = 0^\circ$ and 180° and the largest angle for the T forms at $\phi = 90^\circ$ and 270° (see Figure 4b). This also supports the stability of the latter conformations.

4 Analysis of NMR Spin-Spin Coupling Constants

There are 26 different NMR SSCCs for THF: two ${}^n\text{J}({}^{17}\text{O}-{}^{13}\text{C})$, two ${}^n\text{J}({}^{17}\text{O}-{}^1\text{H})$, four ${}^n\text{J}({}^{13}\text{C}-{}^{13}\text{C})$, eight ${}^n\text{J}({}^{13}\text{C}-{}^1\text{H})$, and ten ${}^n\text{J}({}^1\text{H}-{}^1\text{H})$ SSCCs. Because of the small natural abundance of ${}^{17}\text{O}$ and its large quadrupole moment, ${}^{17}\text{O}$ SSCCs are difficult to measure and only a relatively small number of reliable SSCCs involving ${}^{17}\text{O}$ is available [66]. Nevertheless, it is still interesting to investigate the conformational dependence of SSCCs involving ${}^{17}\text{O}$ and test their use as descriptors of the electronic structure of THF. In this work, we provide the full set of all 26 SSCCs of THF.

For cyclopentane [12], we showed that ${}^3\text{J}(\text{HCCH})$ expressed as a function of the associated dihedral angle $\tau(\text{HCCH})$ can only be described by two rather than one Karplus relationship because one $\tau(\text{HCCH})$ value can lead to two significantly different ${}^3\text{J}(\text{HCCH},\text{cis})$ values. For THF, even six Karplus relationships are needed to represent all ${}^3\text{J}(\text{HCCH},\text{cis})$ values for fragments H6C2C3H8 and H8C3C4H10 as a function of the associated dihedral angle $\tau(\text{HCCH})$ in an accurate way. These problems vanish when SSCCs J are expressed as functions of the ring puckering coordinates according to Eq.s (7) or (9).

In Table 4, the Fourier expansion coefficients of Eq. (9) are given for all 26 SSCCs of THF. The calculated average SSCCs $\langle {}^n\text{J} \rangle$ based on B3LYP and MBPT(2) geometries are listed in Table 5 and compared with measured J values and the corresponding SSCCs of cyclopentane [12]. Karplus relationships (9) are shown for selected SSCCs in Figure 6.

In the following, we will discuss the SSCCs of THF (Tables 4 and 5) separately where the emphasis will be on those SSCCs that can be used for the determination of the conformation of THF and its derivatives. The SSCCs of THF are dominated by the FC contribution whereas the PSO, DSO, and SD contributions make small but significant contributions (≤ 3 Hz, e.g. for the one-bond SSCCs). Hence, the calculation of these terms is absolutely necessary to obtain reliable J values, however the dependence of J on the puckering coordinates can be rationalized by concentrating on the FC term only.

One-Bond Coupling Constant ${}^1\text{J}(\text{OC})$. This SSCC is dominated by the FC term, which changes significantly with ϕ . However, the changes in PSO+DSO+SD are opposite to that of the FC contribution so that the total SSCC changes by only 0.4 Hz from 26.1 ($\phi = 18, 198^\circ$) to 26.6 Hz ($\phi = 126, 306^\circ$). Hence, the total SSCC is of little use for the conformational analysis.

One-Bond Coupling Constants ${}^1\text{J}(\text{CC})$. The position of the electronegative O atom has little effect on ${}^1\text{J}(\text{CC})$ constants. The calculated SSCC value is 34.0 Hz for $\langle {}^1\text{J}(\text{C2C3}) \rangle$ and 34.2 Hz for $\langle {}^1\text{J}(\text{C3C4}) \rangle$, respectively, which are comparable to the measured values for propane (34.6) [30], cyclohexane(32.7) [30] and the calculated value of $\langle {}^1\text{J}(\text{CC}) \rangle$ for cyclopentane (34.0 Hz [12]). The variation of ${}^1\text{J}(\text{C3C4})$ ($\Delta = 3.7$ Hz) is much larger than the changes in ${}^1\text{J}(\text{C2C3})$ ($\Delta = 1.1$ Hz),

which is opposite to the changes in the corresponding bond lengths (see discussion in previous section). The changes in the one-bond SSCCs can however be directly explained considering the products $\rho_s(\text{C,C})$ of the densities at the nuclei (see Eq. 6). This will be large if exchange repulsion (bond eclipsing) increases. A large density at the site of the nuclei guarantees a stronger transmission of spin polarization from one nucleus to the other.

Table 4. Fourier expansion coefficients for the SSCCs of THF. ^a

Parameter	Definition	A ₀	B ₁ cos ϕ	B ₂ cos 2 ϕ	B ₃ cos 3 ϕ	B ₄ cos 4 ϕ	B ₅ cos 5 ϕ	C ₁ sin ϕ	C ₂ sin 2 ϕ	C ₃ sin 3 ϕ	STD
¹ J(CH)	C2H6	142.57	3.03	-0.38	-0.06	0.04	0.03	1.91	0.77	0.03	0.04
¹ J(CH)	C3H8	130.89	1.01	0.26	-0.05		0.02	-2.09	-0.01	0.07	0.04
¹ J(CC)	C3C4	34.35		1.83							0.02
¹ J(CC)	C2C3	34.06		0.43		-0.01			0.28		0.02
¹ J(OC)	O1C2	26.41		-0.16		-0.01			0.19		0.04
² J(CC)	C2O1C5	0.87		0.52		0.07					0.00 ₄
² J(CC)	C2C3C4	0.41		-0.83		0.03			0.50		0.04
² J(OC)	O1C2C3	0.22		-0.69		0.05			0.14		0.02
² J(OH)	O1C2H6	-8.62	-4.96	0.54	0.43	-0.02	-0.02	-1.74	-0.01	0.31	0.02
² J(CH)	C2C3H8	-1.52	-1.44	-0.22	-0.21	-0.02		-3.00	-0.10	-0.10	0.00 ₇
² J(CH)	C3C2H6	-0.64	-0.64	0.49	0.20	-0.04		0.11	0.23	0.04	0.03
² J(CH)	C3C4H10	-2.76	-0.60		-0.06	0.02	0.01	0.39	-0.31	0.16	0.01
² J(HH)	H6C2H7	-8.78		-0.45		0.03			-0.07		0.05
² J(HH)	H8C3H9	-12.03		-0.03		-0.02			0.26		0.05
³ J(OH)	O1C2C3H8	-1.20	0.95	0.25	0.06	0.07	0.02	1.80	-0.55	0.25	0.04
³ J(CH)	C2C3C4H10	2.92	-0.31	-1.15	-0.20	-0.08	-0.03	3.85	-0.17	0.39	0.05
³ J(CH)	C2O1C5H12	4.12	5.54	1.26	-0.33	0.02		-2.12	-1.14	0.52	0.07
³ J(CH)	C4C3C2H6	2.95	2.34	0.30	0.06	0.03	0.01	2.10	1.88	-0.38	0.02
³ J(HH)	H6C2C3H8	7.37	0.42	0.54	0.16	-0.12		1.50	-2.09	0.08	0.03
³ J(HH)	H8C3C4H10	8.65	0.75	2.41	0.18	0.11					0.01
³ J(HH)	H6C2C3H9	5.34	-3.44	-0.10	-0.77	0.09		-4.93	0.20	0.23	0.06
³ J(HH)	H8C3C4H11	5.44		-0.93		-0.14		6.58		0.77	0.02
⁴ J(HH)	H6C2O1C5H12	-0.20	-0.26	0.33	0.27	-0.05	-0.03				0.00 ₅
⁴ J(HH)	H6C2C3C4H10	-0.17	0.21	-0.12	-0.10	-0.01	-0.01	0.13	0.30	0.02	0.00 ₃
⁴ J(HH)	H6C2O1C5H13	-0.58		-0.41		0.14		-0.34		0.12	0.01
⁴ J(HH)	H6C2C3C4H11	-0.61	-0.11	-0.02	0.01	-0.01	0.01	0.03	0.03	-0.03	0.04

a) The Fourier expansion given in Eq. (9) was used. Coefficients B_i and C_j associated with cos (i ϕ) and sin (j ϕ), respectively, are listed. Constant A₀ corresponds to the average parameter $\langle {}^n\text{J} \rangle$ in the case of free pseudorotation. All SSCCs ⁿJ in Hz. For the numbering of atoms, see Figures 1 and 2.

Table 5. Comparison of calculated and measured $\langle^nJ\rangle$ values of THF. ^a

SSCC	$\langle^nJ\rangle$		exp.	$\langle^nJ\rangle$ cyclopentane ^d
	MP2	B3LYP		
¹ J(C2H6)	141.47	142.60	144.6 ^b	127.61
¹ J(C3H8)	130.13	130.88	132.2 ^b	127.61
¹ J(C3C4)	34.27	34.23		34.05
¹ J(C2C3)	34.01	34.04		34.05
¹ J(O1C2)	25.51	26.42		
² J(C2O1C5)	0.93	0.84		2.33
² J(C2C3C4)	0.29	0.47		2.33
² J(O1C2C3)	0.09	0.27		
² J(O1C2H6)	-8.39	-8.65		
² J(C2C3H8)	-1.63	-1.50		-2.58
² J(C3C2H6)	-0.73	-0.67		-2.58
² J(C3C4H10)	-2.83	-2.76		-2.58
² J(H6C2H7)	-8.55	-8.75		-12.41
² J(H8C3H9)	-11.63	-12.03		-12.41
³ J(O1C2C3H8)	-1.33	-1.21		
³ J(C2C3C4H10)	3.13	2.99		3.92
³ J(C2O1C5H12)	4.17	4.04		3.92
³ J(C4C3C2H6)	3.20	2.93		3.92
³ J(H6C2C3H8,cis)	7.19	7.33	7.94 ^c	7.69
³ J(H8C3C4H10,cis)	8.24	8.51	8.65 ^c	7.69
³ J(H6C2C3H9,trans)	5.29	5.35	6.14 ^c	5.61
³ J(H8C3C4H11,trans)	5.47	5.50	6.25 ^c	5.61
⁴ J(H6C2O1C5H12,cis)	-0.16	-0.23		0.10
⁴ J(H6C2C3C4H10,cis)	-0.12	-0.16		0.10
⁴ J(H6C2O1C5H13,trans)	-0.59	-0.55		-0.57
⁴ J(H6C2C3C4H11,trans)	-0.59	-0.61		-0.57

a) All SSCCs $\langle^nJ\rangle$ in Hz. b) Taken from ref. 30. c) Taken from ref. 29. d) Taken from Ref. 12.

In this respect, exchange repulsion effects increase both the FC term of the SSCCs and the bond length, i.e. the latter do not directly influence the one-bond SSCC.

One-Bond Coupling Constants $^1J(\text{CH})$. In contrast to $^1J(\text{CC})$, $^1J(\text{CH})$ exhibits a strong dependence on the position of the O atom. The average SSCC values are 142.6 Hz for $^1J(\text{C2H6})$ and 130.9 Hz for $^1J(\text{C3H8})$, respectively, which are in reasonable agreement with measured values of 144.6 for $^1J(\text{C2H6})$ and 132.2 for $^1J(\text{C3H8})$ (see Table 5 and Figure 6a). The difference of 12 Hz between $\langle ^1J(\text{C2H6}) \rangle$ and $\langle ^1J(\text{C3H8}) \rangle$ is a result of the inductive effect of the O atom [30]. Analysis of the *s*-density reveals that at C2 (bond C2H6: $\simeq 0.096$ electron) it is significantly larger than the *s*-density at C3 (bond C3H8: $\simeq 0.070$ electron; see Figure 5). $^1J(\text{C2H6})$ changes by 7.3 Hz from 145.4 ($\phi = 36^\circ$) to 138.1 Hz ($\phi = 216^\circ$). This decrease is caused by a change in the position of bond C2H6 relative to the mean plane of the ring. Calculating the ring substituent orientations according to Cremer [36] reveals that C2H6 is in the equatorial position for $\phi = 36 \pm 18^\circ$ and in the axial position for $\phi = 216 \pm 72^\circ$. In the latter situation, the Perlin effect (the magnetic analogue of the anomeric effect) [5,67] decreases $^1J(\text{C2H6})$ and enlarges the difference $^1J(\text{CH}_{eq}) - ^1J(\text{CH}_{ax})$. The Perlin effect is well-known for the $^1J(\text{CH})$ constants of heterocyclohexanes [68] and, obviously, plays also a role in five-membered rings with hetero atoms.

Geminal Coupling Constants $^2J(\text{OCC})$ and $^2J(\text{CCC})$. The three $^2J(\text{X,C})$ constants possess positive average values: 0.3 Hz for $\langle ^2J(\text{O1C2C3}) \rangle$, 0.5 Hz for $\langle ^2J(\text{C2C3C4}) \rangle$, and 0.8 Hz for $\langle ^2J(\text{C2O1C5}) \rangle$. For the purpose of explaining the ϕ -dependence of these SSCCs, one has to consider that there are two coupling paths as reflected by notations such as $^{2+3}J(\text{XCC},\text{XCCC})$ with X = C or O. The two-bond contribution of $^2J(\text{CXC})$ and $^2J(\text{XCC})$ are almost constants during pseudorotation. Hence, the total coupling constants depend on the changes in the three-bond contributions, which in turn correlate with the dihedral angle of the corresponding fragments XCCC and CXCC in the sense that a larger deviation of the dihedral angle from 0° leads to a smaller value of the coupling constant (see Figure 7).

Geminal Coupling Constants $^2J(\text{OCH})$ and $^2J(\text{CCH})$. The calculated value of the SSCC $\langle ^2J(\text{C3C4H10}) \rangle$ is -2.8 Hz and agrees well with $\langle ^2J(\text{CCH}) \rangle$ for cyclopentane (-2.6 Hz, Table 1). The inductive effect of an O atom leads to a positive contribution of 1 - 2 Hz depending on the position of O and the relative orientation of CO and CH bond [30]. This is also reflected by $\langle ^2J(\text{C3C2H6}) \rangle = -0.7$ Hz and $\langle ^2J(\text{C2C32H8}) \rangle = -1.5$ Hz. Of the four $^2J(\text{XCH})$ SSCCs, $^2J(\text{C2C3H8})$ and $^2J(\text{O1C2H6})$ are most sensitive to the pseudorotational phase angle ϕ (see Figure 6b). $^2J(\text{C2C3H8})$ changes by 6.3 Hz from -4.6 ($\phi = 36^\circ, 54^\circ$) to 1.7 Hz ($\phi = 252^\circ$) where its value depends on the relative orientation of the CO bond as reflected by $\tau(\text{O1C2C3H8})$ (the larger τ , the more positive $^2J(\text{C2C3H8})$; see Figures 4d and 6b). Similar effects have been reported [5,67] and frequently utilized to study the conformation of important biological compounds [68]. $^2J(\text{O1C2H6})$ changes by 10 Hz from -13.4 Hz ($\phi = 54^\circ$) to -3.4 Hz ($\phi = 198^\circ$). The *s*-character of the hybrid orbital of bond C2H6 influences $^2J(\text{O1C2H6})$, $^1J(\text{C2H6})$, and $^2J(\text{H6C2H7})$. An increase in the *s*-character of $\text{sp}^x(\text{C2H6})$ leads to a more negative $^2J(\text{O1C2H6})$ SSCC (see Figures 5 and

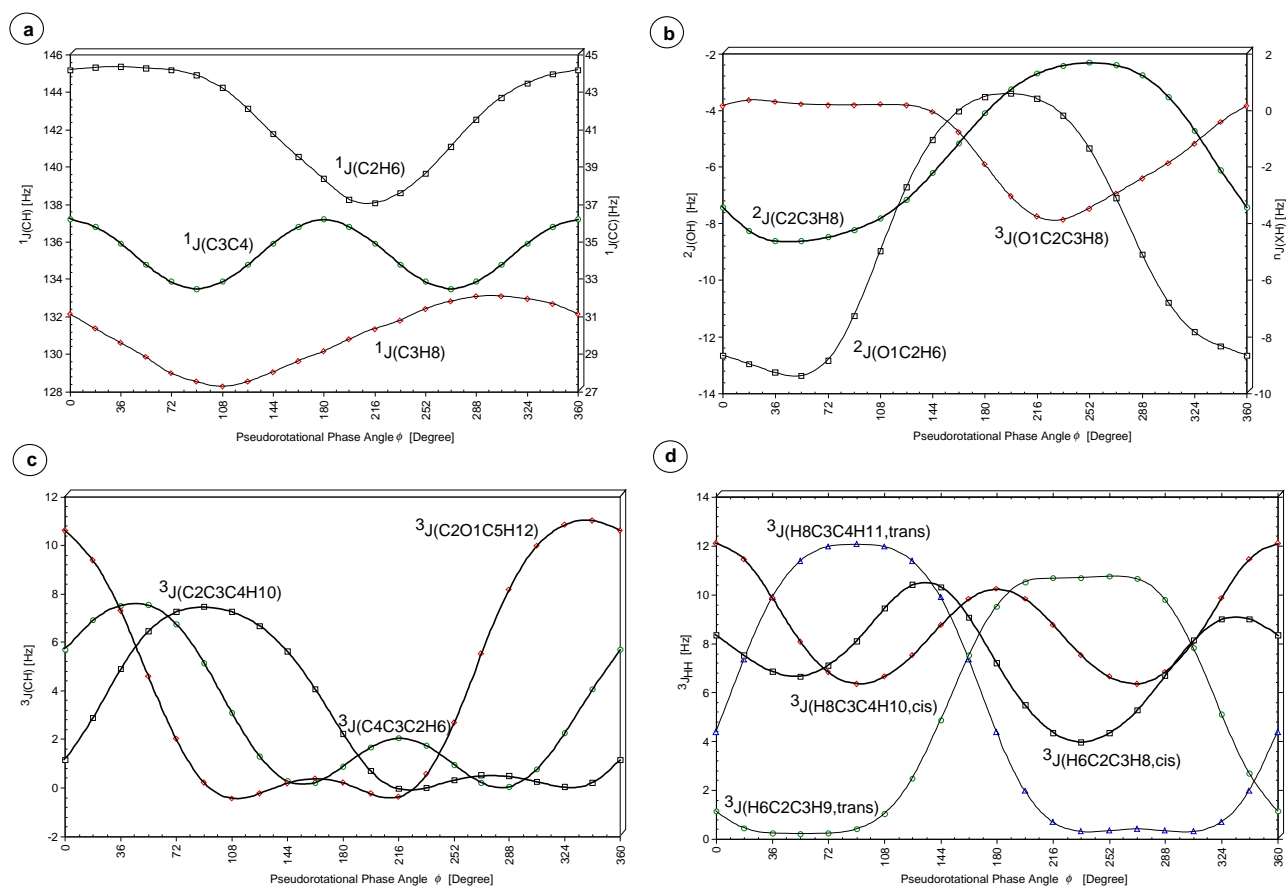


Figure 6: Calculated SSCCs nJ as a function of the pseudorotational phase angle ϕ . (a) One-bond SSCCs ${}^1J(\text{C2H6})$, ${}^1J(\text{C3C4})$ and ${}^1J(\text{C3H8})$. (b) ${}^2J(\text{O1C2H6})$, ${}^2J(\text{C2C3H8})$ and ${}^3J(\text{O1C2C3H8})$. (c) Vicinal SSCCs ${}^{13}\text{C}$ - ${}^1\text{H}$ SSCCs ${}^3J(\text{C2O1C5H12})$, ${}^3J(\text{C2C3C4H10})$ and ${}^3J(\text{C4C3C2H6})$. (d) Vicinal SSCCs ${}^1\text{H}$ - ${}^1\text{H}$ SSCCs ${}^3J(\text{H6C2C3H8,cis})$, ${}^3J(\text{H6C2C3H9,trans})$, ${}^3J(\text{H8C3C4H10,cis})$, and ${}^3J(\text{H8C3C4H11,trans})$. For the numbering of atoms, see Figures 1 and 3. The coefficients of the Fourier expansions ${}^nJ(\phi)$ are listed in Table 4. All calculations at B3LYP/6-31G(d,p) geometries.

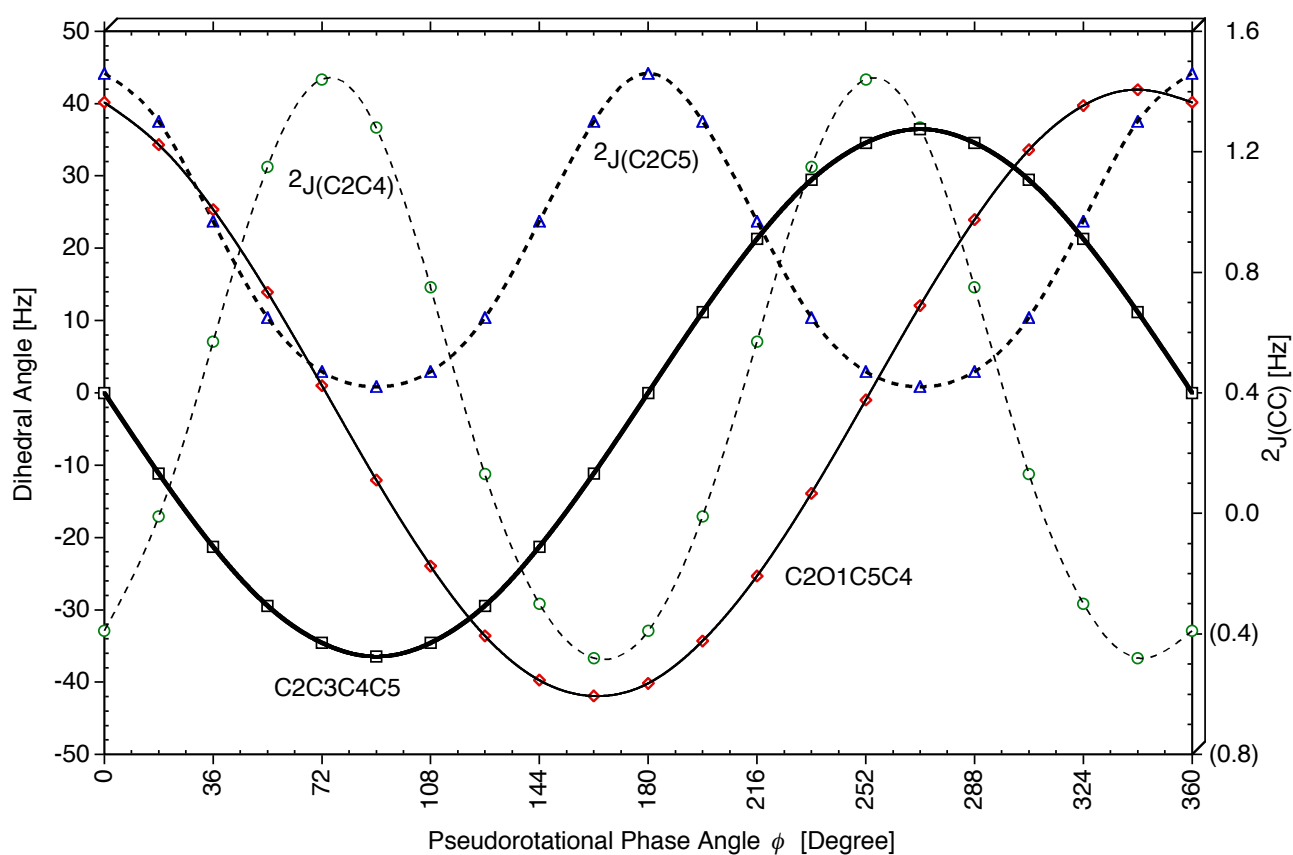


Figure 7: Calculated SSCCs ${}^2J(\text{CXC})$ ($X = \text{O}$ or C) as a function of the pseudorotational phase angle ϕ (dashed lines). Also shown is the relationship of SSCCs ${}^2J(\text{CXC})$ to a possible three-bond coupling path by giving the dihedral angles associated to this path also as a function of the pseudorotational phase angle ϕ (solid lines). In this way, ${}^2J(\text{C2O1C5})$ is associated with dihedral angle $\tau(\text{C2C3C4C5})$ and ${}^2J(\text{C2C3C4})$ with dihedral angle $\tau(\text{C2O1C5C4})$. The more the dihedral angle deviates from 0° , the smaller the SSCCs become.

6b). If ^{17}O SSCCs could be measured, $^2\text{J}(\text{O1C2H6})$ would be an useful conformational probe.

Geminal Coupling Constants $^2\text{J}(\text{HCH})$. The dependence of $^2\text{J}(\text{HCH})$ on the hybridisation degree of the C atom and the impact of an electronegative atom are well known [1,4,5,30]. The calculated values of $\langle ^2\text{J}(\text{H6C2H7}) \rangle$ (-8.7 Hz, Table 5) and $\langle ^2\text{J}(\text{H8C2H9}) \rangle$ (-12.0 Hz) reflect these trends. $\langle ^2\text{J}(\text{H8C2H9}) \rangle$ agrees well with the calculated $\langle ^2\text{J}(\text{HCH}) \rangle$ value for cyclopentane (-12.4 Hz, Table 5).

Vicinal Coupling Constants $^3\text{J}(\text{OCCH})$, $^3\text{J}(\text{CCCH})$. All $^3\text{J}(\text{XCCH})$ couplings depend strongly on the pseudorotational phase angle ϕ (see Figure 6c). The values of $\langle ^3\text{J}(\text{C, H}) \rangle$, are all positive ($^3\text{J}(\text{C4C3C2H6})$: 2.9; $^3\text{J}(\text{C2C3C4H10})$: 3.0; $^3\text{J}(\text{C2O1C5H12})$: 4.0 Hz, Table 5) and comparable to the corresponding cyclopentane value of 3.9 Hz (Table 5). The O atom as an external substituent of the CCH unit decreases the SSCC, however O in the ether position increases the SSCC [30]. The value of $\langle ^3\text{J}(\text{OCCH}) \rangle$ is -1.2 Hz whereas $^3\text{J}(\text{OCCH})$ varies by 4.3 Hz from -3.9 ($\phi = 234^\circ$) to 0.4 Hz ($\phi = 36^\circ$) and thus reflects the corresponding changes in $\tau(\text{O1C2C3H8})$ (Figure 4d). Variations in the vicinal SSCCs by 7.5 Hz ($^3\text{J}(\text{C2C3C4H10})$), 11.5 Hz ($^3\text{J}(\text{C2O1C5H12})$), and 7.6 Hz ($^3\text{J}(\text{C4C3C2H6})$, Figure 6c) can be explained by considering both the *s*-character of CH (or CC) bonds and the dihedral angle $\tau(\text{CCCH})$ (see also Ref. 12).

Vicinal Coupling Constants $^3\text{J}(\text{HCCH})$. The SSCC $^3\text{J}(\text{H8C3C4H10,cis})$ possesses a similar dependence on ϕ than the corresponding SSCC in cyclopentane [12], adopting large values for $\tau(\text{H8C3C4H10}) = 0^\circ$ (12.1 and 10.2 Hz at $\phi = 0^\circ$ and 180° ; Figure 6d) and smaller values for $\tau(\text{H8C3C4H10}) = 40.7^\circ$ (6.4 Hz for $\phi = 90^\circ$ and 270°). The difference $\Delta = 1.86$ Hz between the *endo*- $^3\text{J}(\text{H8C3C4H10,cis})$ ($\phi = 180^\circ$) and the *exo*- $^3\text{J}(\text{H8C3C4H10,cis})$ value ($\phi = 0^\circ$) is another example for the *Barfield transmission effect* [70,71], which has been studied by various authors and which has been explained in different ways [69-71]. Noteworthy in this connection is that differences in SSCC due to the Barfield transmission effect are automatically covered when the SSCCs are expanded as functions of the puckering coordinates (see Figure 6d).

An accurate description of the variation in $^3\text{J}(\text{H8C3C4H10,cis})$ during pseudorotation requires $\cos 3\phi$ and $\cos 4\phi$ terms (standard deviation 0.01 Hz; see Table 4). The average value of SSCC $^3\text{J}(\text{H8C3C4H10,cis})$ is calculated to be 8.51 Hz, which is in good agreement with the measured value of 8.65 Hz [29]. For cyclopentane the corresponding SSCC is 0.8 Hz larger (see Table 5).

The Karplus relationship $^3\text{J}(\text{H6C2C3H8,cis}) = ^3\text{J}(\phi)$ is shifted by 216° relative to that for $^3\text{J}(\text{H8C3C4H10,cis})$ (see Figure 6d). It has a similar, however somewhat asymmetrical shape (caused by a similar asymmetry in $\tau(\text{H6C2C3C8})$) where J varies by 6.4 Hz from 4 Hz ($\phi = 234^\circ$) to 10.4 Hz ($\phi = 126^\circ$). Again, the electronegative O atom leads to a lower $\langle ^3\text{J}(\text{H6C2C3H8,cis}) \rangle$ value (7.33 Hz, Table 5), which is in reasonable agreement with the experimental value of 7.94 Hz [29]. The Barfield transmission effect is now smaller as reflected by an *exo-endo* difference of 1.33 Hz (*endo*, $\phi = 324^\circ$, 8.99 Hz; *exo*, $\phi = 144^\circ$, 10.32 Hz).

As in the case of cyclopentane, the dependence of ${}^3J(\text{HCCH,trans})$ on pseudorotation is considerably different from that observed for ${}^3J(\text{HCCH,cis})$ (Figure 6d). Utilizing the ϕ -dependence of ${}^3J(\text{H8C3C4H11})$, the conformational space can be partitioned into several regions: ${}^3J(\text{H8C3C4H11})$ adopts values ≥ 10 Hz for $36^\circ \leq \phi \leq 144^\circ$; it becomes ≤ 2 Hz for $198^\circ \leq \phi \leq 342^\circ$, and takes intermediate values in the remaining regions. The Karplus relationships for ${}^3J(\text{HCCH,trans})$ are given in Table 4. The values of $\langle {}^3J(\text{HCCH,trans}) \rangle$ are 5.50 for ${}^3J(\text{H8C3C4H11})$ and 5.35 Hz for ${}^3J(\text{H6C2C3H9})$, which are 0.7 - 0.8 Hz smaller than the measured values of 6.25 and 6.14 Hz [29], respectively. We note that as in the case of cyclopentane the average cis-SSCCs are better described than the average trans-SSCCs. Since the latter are largely insensitive to ring puckering, this deviation is due to shortcomings of the method (lack of higher order correlation effects). We note in this connection that $\langle {}^3J(\text{HCCH,trans}) \rangle$ is also calculated somewhat too small for alkanes and alkenes irrespective of the basis set.

Long Range Coupling Constants ${}^4J(\text{HCCCH})$. The four long-range SSCCs (two cis- + two trans- ${}^4J(\text{HCCCH})$ constants, see Tables 4 and 5) change only slightly (≤ 1.5 Hz) during pseudorotation. Average values are -0.23 Hz for $\langle {}^4J(\text{H6C2O1C5H12}) \rangle$, -0.16 Hz for $\langle {}^4J(\text{H6C2C3C4H19}) \rangle$, -0.55 Hz for ${}^4J(\text{H6C2O1H13})$, and -0.61 Hz for ${}^4J(\text{H6C2C3C4H11})$.

5 A General Karplus Relationship for Puckered Rings

In this section, we discuss the more general Karplus relationship $J(q,\phi)$ given in Eq. (7), which leads to a three-dimensional (3D) surface for the SSCC. If function (7) is known, it can be used to describe the conformation of THF and its derivatives more accurately in terms of the mode and the degree of ring puckering.

In the case of THF, the puckering amplitude is largely constant along the pseudorotational path (Table 1) so that one can discuss the dependence of J on q and ϕ separately. For the purpose, of evaluating the q -dependence of the SSCCs, we repeated geometry optimizations at the B3LYP/6-31G(d,p) level of theory for fixed values of q , varying q in the range from 0.33 to 0.41 Å. Subsequent calculation of the SSCCs for the new set of geometries made it possible to derive the coefficients in Eq.s (8a), (8b), and (8c) truncating the power series in q after the quadratic term (see below). Insertion into Eq. (7) led to the general Karplus relationship $J(q,\phi)$. As a representative example, we discuss here results for SSCC ${}^3J(\text{H8C3C4H10,cis})$.

The Fourier expansion coefficients B_k and C_k are listed in Table 6 for each q value chosen. The calculated 3D-surface of the ${}^3J(\text{H8C3C4H10,cis})$ SSCC is shown in Figure 8.

As stated in section 2, the Fourier coefficient $A_0(q)$ approaches for $q \rightarrow 0$ the value of the SSCC ${}^3J(\text{H8C3C4H10,cis})$ for the planar form. All other coefficients become zero for $q = 0$. The experience obtained in this work suggests that a truncation after the quadratic term is sufficient

to give a reliable account of the dependence of the power series coefficients A_{0l} , B_{kl} and C_{kl} on q . Figure 8 shows that ${}^3J(\text{H8C3C4H10,cis})$ decreases rapidly with increasing q where the decrease for the C_2 -symmetrical T forms is stronger than for the C_s -symmetrical E forms. It can also be seen that in the latter case the SSCC is always larger for $\phi = 0^\circ$ than for $\phi = 180^\circ$ and that the difference becomes smaller for q approaching 0 while ${}^3J(\text{H8C3C4H10,cis})$ converges to 12.48 Hz, the SSCC of the planar form. The value of $\langle {}^3J(\text{H8C3C4H10,cis}) \rangle$ also exhibits a significant dependence on q , which in turn can be used for the determination of the puckering amplitude q as discussed in Ref. 12.

Table 6. Fourier expansion coefficients (in Hz) of ${}^3J(\text{H8C3C4H10})$ for different q values.

q	A	B1 $\cos(\phi)$	B2 $\cos(2\phi)$	B3 $\cos(3\phi)$	B4 $\cos(4\phi)$
0.00	12.48				
0.33	9.30	0.78	2.03	0.13	0.07
0.35	8.98	0.77	2.22	0.15	0.09
0.371 ^a	8.65	0.75	2.41	0.18	0.11
0.39	8.34	0.74	2.60	0.20	0.13
0.41	8.02	0.71	2.77	0.22	0.16

a) Optimized puckering amplitude (see Table 1.)

For the vicinal proton,proton SSCCs of THF, general Karplus relationship $J(q,\phi)$ were determined and used in connection with the corresponding experimental values to determine in a least square sense that puckering amplitude q of THF that leads to the best agreement between measured and calculated averaged SSCCs. As shown in Figure 9, a q -value of 0.352 Å was obtained in this way (predominantly determined by ${}^3J(\text{HCCH,cis})$, see Figure 9), which is clearly smaller than the gas phase value of 0.396 Å (Table 1). The difference of 0.044 Å reflects vibrational and environmental effects on the puckering amplitude q where one has to consider that the vicinal proton,proton SSCCs of THF were measured in CHCl_3 [29]. While the large amplitude vibration along the pseudorotational path does not change q very much, the second large amplitude vibration perpendicular to the mean plane of the ring decreases q because of the relatively low barrier to inversion (4 kcal/mol, Table 1). Molecular interactions in condensed phases seem to flatten the ring as was also observed in the X-ray [23] and the neutron diffraction study [24] of THF. We note

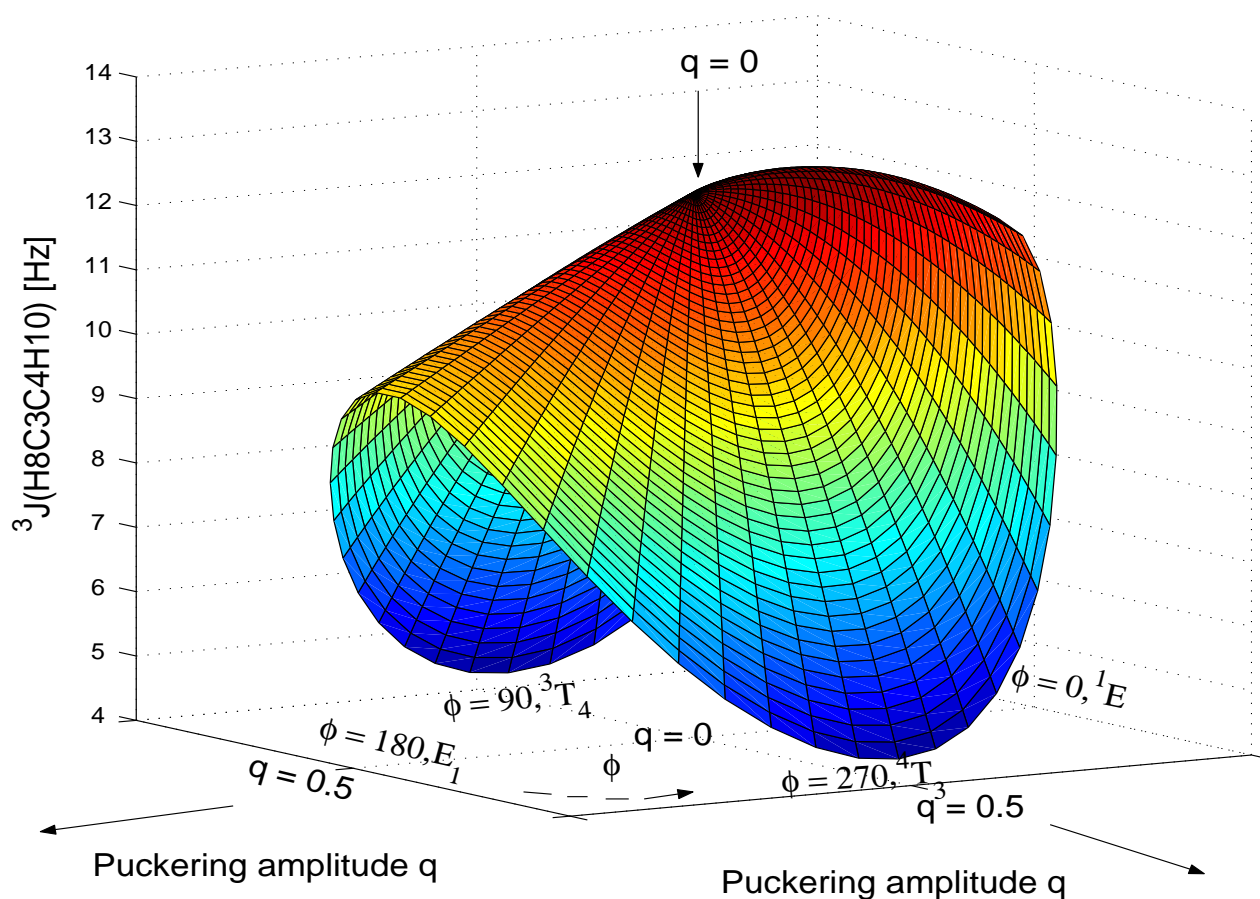


Figure 8: Perspective drawing of the three-dimensional surface $J(q, \phi)$ of SSCC ${}^3J(\text{H8C3C4H10, cis})$ of tetrahydrofuran. The SSCC of the planar form with $q = 0$ is located at the maximum. The direction of radial coordinate q and the angular coordinate ϕ is indicated. Compare with Figure 1. The drawing is cutoff for $q > 0.5 \text{ \AA}$.

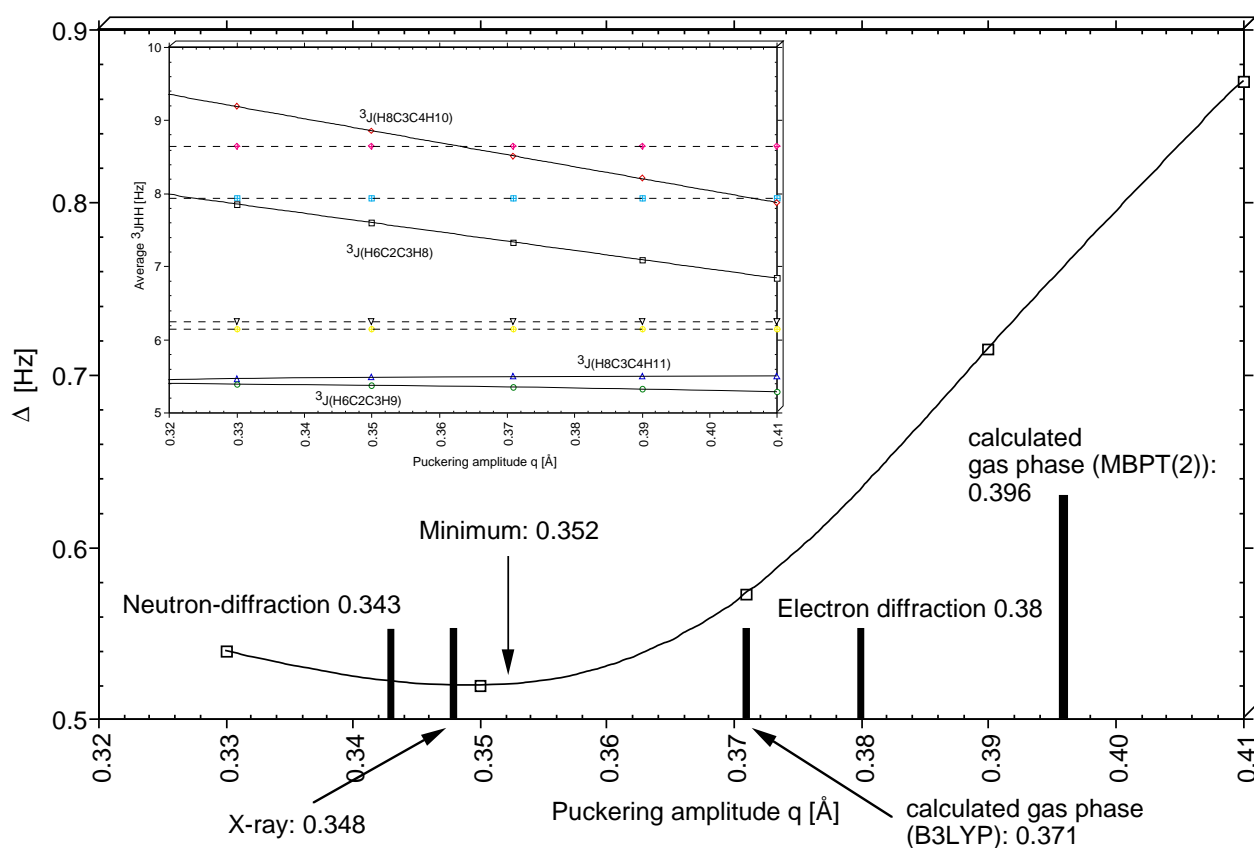


Figure 9: The total deviation Δ of calculated from experimental SSCCs $\langle ^3J(HCCH) \rangle$ is given as a function of q . The minimum determines the best q value. It is compared with the q values from other sources. In the insert, the dependence of the calculated SSCCs $\langle ^3J(HCCH) \rangle$ of THF on the puckering amplitude q is given. Experimental values (dashed lines) are given for comparison.

that the q-values obtained in the solid state (0.348 and 0.343 Å; Table 3) are close to the q-value determined with the help of the vicinal SSCCs. Hence, a realistic puckering amplitude of THF in solution should be close to 0.35 Å.

6 Conclusions

The following conclusions can be drawn from this work.

- 1) MBPT(2)/cc-pVTZ provides a reliable description of the conformational behavior of THF. THF is a slightly hindered pseudorotor with a constant puckering amplitude of 0.396 Å; the global minima correspond to the C_2 -symmetrical T forms at $\phi = 90$ and 270° . The pseudorotational and inversion barriers $\Delta H(298)$ are 0.22 and 4.15 kcal/mol, respectively, which agree well with the available spectroscopic data.
- 2) A fourfold pseudorotational potential for THF as suggested by microwave spectroscopic investigations [20,21] is not confirmed by the quantum chemical calculations. Analysis of the electronic structure of THF along the pseudorotational path clearly indicates that the T forms at $\phi = 90$ and 270° are most stable while the E forms at $\phi = 0$ and 180° occupy the first order saddle points of the CES. We note that the microwave spectroscopic results strongly depend on the constrained THF model used in the investigation and suggest that these investigations should utilize THF models based on the accurate geometries provided in this work.
- 3) B3LYP/6-31G(d,p) calculations are almost as reliable as MBPT(2)/cc-pVTZ results in the case of THF. This result is in so far important as it provides a basis to investigate pseudorotation of ribose and other biochemically interesting ring compounds at the DFT level of theory. In view of the coupling of this mode with the internal rotation of the substituents of ribose such an investigation would become too expensive at the MBPT(2)/cc-pVTZ level of theory.
- 4) CPDFT/B3LYP calculations with the [6s,4p,1d/3s,1p] basis set provide SSCCs in good agreement with the available experimental values for THF and the known SSCCs for cyclopentane. The influence of the O atom on SSCCs involving ^{13}C and ^1H is in line with observations made for acyclic O-containing compounds [30].
- 5) Karplus relationships ${}^n\text{J}(\phi)$ and ${}^n\text{J}(\text{q},\phi)$ are established for all 26 SSCCs of THF. Since all internal coordinates of THF are described in the same way, the analysis of the SSCCs in terms of geometrical parameters is straightforward. Also, SSCCs $\langle {}^n\text{J} \rangle$ averaged over the pseudorotational mode so that they become directly comparable to measured SSCCs, have been calculated. Magnitude and sign of the $\langle {}^n\text{J} \rangle$ values agree well with the corresponding values found for cyclopentane [12] provided the influence of the O atom is considered.
- 6) In Figure 6, those SSCCs are identified that strongly vary during pseudorotation. It has been shown that in particular the vicinal SSCCs, if accurately measured, make it possible to exactly

determine the conformation of the THF molecule in solution. A puckering amplitude of 0.352 Å was determined in this way.

Work is in progress to develop a procedure that utilizes the Karplus relationships established in this work to determine the conformation of substituted THF compounds with the help of measured SSCCs. This method and the results summarized in this article provide an excellent platform for analyzing the conformational behavior of biochemically interesting molecules such as ribose, 2'-deoxyribose, proline, etc.

7 Acknowledgment

This work was supported by the Swedish Natural Science Research Council (NFR). Calculations were done on the supercomputers of the Nationellt Superdatorcentrum (NSC), Linköping, Sweden. DC thanks the NSC for a generous allotment of computer time.

References

- [1] Grant, D. M.; Harris, R. K., Edt.s, *Encyclopedia of Nuclear Magnetic Resonance*; Wiley: Chichester, UK, 1996, Vol 1-8.
- [2] Kowalewski, J. Calculations of Nuclear Spin-Spin Coupling Constants. *Prog. NMR Spectrosc.* **1977**, *11*, 1-78.
- [3] Kowalewski, J. Calculations of Nuclear Spin-Spin Couplings. *Ann. Rep. NMR Spectrosc.* **1982**, *12*, 81-176.
- [4] Contreras, R. H.; Facelli, J. C. Advances In Theoretical Physical Aspects of Spin-Spin Coupling Constants. *Ann. Rep. NMR Spectrosc.* **1993**, *27*, 255-356.
- [5] Contreras, R. H.; Peralta, J.E. Angular Dependence of Spin-Spin Coupling Constants. *Prog NMR Spectrosc.* **2000**, *37*, 321-425.
- [6] Karplus, M.; Anderson, D. H. Valence-Bond Interpretation of Electron-Coupled Nuclear Spin Interactions; Application to Methane. *J. Chem. Phys.* **1959**, *30*, 6-10.
- [7] Karplus, M. Contact Electron-Spin Coupling of Nuclear Magnetic Moments. *J. Chem. Phys.* **1959**, *30*, 11-15.
- [8] Karplus, M. Vicinal Proton Coupling in Nuclear Magnetic Resonance. *J. Am. Chem. Soc.* **1963**, *85*, 2870-2871.
- [9] Altona, C. in *Encyclopedia of Nuclear Magnetic Resonance*, Grant, D. M.; Harris, R. K., Edt.s, Wiley:Chichester, UK, 1996, p. 4909.

- [10] Altona, C.; Sundaralingam, M. Conformational Analysis of the Sugar Ring in Nucleosides and Nucleotides. Improved Method for the Interpretation of Proton Magnetic Resonance Coupling Constants. *J. Am. Chem. Soc.* **1973**, *95*, 2333-2344.
- [11] Haasnoot, C. A. G. Conformational Analysis of Six-Membered Rings in Solution: Ring Puckering Coordinates Derived from Vicinal NMR Proton-Proton Coupling Constants. *J. Am. Chem. Soc.* **1993**, *115*, 1460-1468.
- [12] Wu, A.A.; Cremer, D.; Auer, A.A.; Gauss, J. Extension of the Karplus Relationship for NMR Spin-Spin Coupling Constants to Nonplanar Ring Systems: Pseudorotation of Cyclopentane. *J. Phys. Chem. A* **2002**, *106*, 657-667.
- [13] Sychrovsky, V.; Gräfenstein, J.; Cremer, D. Nuclear Magnetic Resonance Spin-Spin Coupling Constants From Coupled Perturbed Density Functional Theory. *J. Chem. Phys.* **2000**, *113*, 3530-3547.
- [14] For a review on the calculation of SSCCs, see Helgaker, T.; Jaszunski, M.; Ruud, K. Ab Initio Methods for the Calculation of NMR Shielding and Indirect Spin-Spin Coupling Constants. *Chem. Rev.* **1999**, *99*, 293-352, and references cited therein.
- [15] Gauss, J.; Stanton, J.F. Analytic CCSD(T) Second Derivatives. *Chem. Phys. Letters* **1997**, *276*, 70-77.
- [16] Szalay, P.G.; Gauss, J.; Stanton, J.F. Analytic UHF-CCSD(T) Second Derivatives. Implementation and Application to the Calculation of the Vibration-Rotation Interaction Constants of NCO and NCS. *Theoret. Chem. Acc.* **1998**, *100*, 5-11.
- [17] Auer, A.A.; Gauss, J. Triple Excitation Effects in Coupled-Cluster Calculations of Indirect Spin-Spin Coupling Constants. *J. Chem. Phys.* **2001**, *115* 1619-1622.
- [18] Lafferty, W.J.; Robinson, D.W.; Louis, R.V.St.; Russell, J.W.; Strauss, H.L. Far-Infrared Spectrum of Tetrahydrofuran: Spectroscopic Evidence for Pseudorotation. *J. Chem. Phys.* **1965**, *42*, 2915-2919.
- [19] Davidson, R.; Warsop, P.A. Energy Levels for Pseudorotation and Their Application to Cyclopentane, Tetrahydrofuran, and 1,3-Dioxolane. *J. Chem. Soc. Faraday Trans II* **1972**, *68*, 1875-1889.
- [20] Engerholm, G.G; Luntz, A.C.; Gwinn, W.D.; Harris, D.O. Ring Puckering in Five-Membered Rings.II. The Microwave Spectrum, Dipole Moment, and Barrier to Pseudorotation in Tetrahydrofuran. *J. Chem. Phys.* **1969**, *50*, 2446-2457.
- [21] Meyer, R.; Lopez, J.C.; Alonso, J.L.; Melandri, S.; Favero, P.G.; Caminati, W. Pseudorotation Pathway and Equilibrium Structure μ From the Rotational Spectrum of Jet-cooled Tetrahydrofuran. *J. Chem. Phys.* **1999**, *111*, 7871-7880.

- [22] Geise, H.J.; Adams, W.J.; Bartell, L.S. Electron Diffraction Study of Gaseous Tetrahydrofuran. *Tetrahedron* **1969**, *25*, 3045-3052.
- [23] Luger, P.; Buschmann, J. Twist Conformation of Tetrahydrofuran in the Crystal Form. *Angew. Chem.* **1983**, *95*, 423-424.
- [24] David, W.I.F.; Ibberson, R.M. A Reinvestigation of the Structure of Tetrahydrofuran by High-Resolution Neutron Powder Diffraction. *Acta Crystallogr., Sect. C* **1992**, *48*, 301-303.
- [25] Cremer, D.; Pople, J.A. Molecular Orbital Theory of the Electronic Structure of Organic Compounds. XXIII. Pseudorotation in Saturated Five-Membered Ring Compounds. *J. Am. Chem. Soc.* **1975**, *97*, 1358-1367.
- [26] Han, S.J.; Kang, Y.K. Pseudorotation in Heterocyclic Five-Membered Rings: Tetrahydrofuran and Pyrrolidine. *J. Mol. Struct. (Theochem)* **1996**, *369*, 157-165.
- [27] Diez, E.; Palma, J.; San-Fabián, J.; Guilleme, J. Effect of the Substituents on the Conformational Behavior of Five-Membered Rings: Application to cis- and trans-2,5-Dimethoxytetrahydrofuran. *J. Comp. Chem.* **1988**, *9*, 189-199.
- [28] Siri, D.; Gaudel, A.; Tordo, P. Conformational Analysis of Five-Membered Rings by Molecular Mechanics: Application to Nitroxides. *Theochem.* **2002**, *582*, 171-185.
- [29] Lambert, J.B.; Papay, J.J.; Khan, S.A.; Kappauf, K.A.; Magyar, E.S. Conformational Analysis of Five-Membered Rings. *J. Am. Chem. Soc.* **1974**, *96*, 6112-6118.
- [30] Kalinowski, H. O.; Berger, S.; Braun, S. ¹³C-NMR-Spektroskopie, Thieme: Stuttgart, 1984.
- [31] Church, T.J.; Carmichael, I.; Serianmi, A.S. 13C-1H and 13C-13C Spin-Coupling Constants in Methyl β -D-Ribofuranoside and Methyl 2-Deoxy- β -D-erythro-pentofuranoside: Correlations with Molecular Structure and Conformation. *J. Am. Chem. Soc.* **1997**, *119*, 8946-8964.
- [32] Jaworski, A.; Ekiel, I.; Shugar, D. Coupling Constants between Cisoidal Protons in Pentose Nucleosides. Limitations of Range of Application of Karplus Relation, and Solution Conformations of β -arabinofuranosyl and β -xylofuranosyl Nucleosides. *J. Am. Chem. Soc.* **1978**, *100*, 4357-4361.
- [33] Jaworski, A.; Ekiel, I. Calculations of Proton NMR Coupling Constants for Conformational Studies of Isomeric Pentofuranosyl Nucleosides. *Int. J. Quant. Chem.* **1979**, *16*, 615-622.
- [34] Cremer, D.; Pople, J. A. General Definition of Ring Puckering Coordinates. *J. Am. Chem. Soc.* **1975**, *97*, 1354-1358.
- [35] Cremer, D.; Szabo, K. J. *Methods in Stereochemical Analysis, Conformational Behavior of Six-Membered Rings, Analysis, Dynamics, and Stereoelectronic Effects*, E. Juaristi, Edt., VCH Publishers, 1995, 59-135.
- [36] Cremer, D. A General Definition of Ring Substituent Positions. *Israel J. Chem.* **1980**, *20*, 12-19.

- [37] Cremer, D. Calculation of Puckered Rings With Analytical Gradients. *J. Phys. Chem.* **1990**, *94*, 5502-5509.
- [38] Cremer, D. On the Correct Usage of the Cremer-Pople Puckering Parameters as Quantitative Descriptors of Ring Shapes - A Reply to Recent Criticism by Petit, Dillen and Geise. *Acta Cryst. B* **1984**, *40*, 498-500.
- [39] Essen, H.; Cremer, D. On the Relationship between the Mean Plane and the Least-squares Plane of an N-Membered Puckered Ring. *Acta Cryst. B* **1984**, *40*, 418-420.
- [40] Cremer, D. Theoretical Determination of Molecular Structure and Conformation. XI. the Puckering of Oxolanes. *Isr. J. Chem.*, **1983**, *23*, 72-84.
- [41] Cremer, D. Theoretical Determination of Molecular Structure and Conformation. *J. Chem. Phys.* **1979**, *70*, 1898-1910; 1911-1927; 1928-1938.
- [42] Stoddard, J.F, *Stereochemistry of Carbohydrates*, Wiley-Interscience: New York, 1971.
- [43] For a recent review see, Cremer, D. Møller-Plesset Perturbation Theory In: *Encyclopedia of Computational Chemistry* Schleyer, P. v R.; Allinger, N. L.; Clark, T.; Gasteiger, J.; Kollman, P.A.; Schaefer, H. F.; Schreiner, P. R.; Edt.s, Wiley: Chichester UK, Vol 3, 1706.
- [44] Dunning Jr, T. H. Gaussian Basis Sets for Use in Correlated Molecular Calculations. I. the Atoms boron through Neon and Hydrogen. *J. Chem. Phys.* **1989**, *99*, 1007-1023.
- [45] Kohn, W.; Sham, L. J. Quantum Density Oscillations in an Inhomogeneous Electron Gas. *Phys.Rev.* **1965**, *137*, 1697-1705.
- [46] For a review on DFT, see, e.g., Parr, R. G.; Yang, W. *International Series of Monographs on Chemistry 16: Density-Functional Theory of Atoms and Molecules*; Oxford University Press: New York, 1989.
- [47] Becke, A. D. Density-Functional Thermochemistry. III. the Role of Exact Exchange. *J. Chem. Phys.* **1993**, *98*, 5648-5652.
- [48] Becke, A. D. Density-Functional Exchange-Energy Approximation With Correct Asymptotic Behavior. *Phys. Rev. A* **1988**, *38*, 3098-3100.
- [49] Lee, C.; Yang, W.; Parr, R. G. Development of the Colle-Salvetti Correlation-Energy Formula into a Functional of the Electron Density. *Phys. Rev. B* **1988**, *37*, 785-789.
- [50] Hariharan, P. C.; Pople, J. A. Influence of Polarization Functions on MO Hydrogenation Energies. *Theoret. Chim. Acta* **1973**,*28*, 213-222.
- [51] McQuarrie, D.A. *Statistical Thermodynamics*, Harper and Row Publishers: New York, 1973.
- [52] Kraka, E.; Gauss, J.; Cremer, D. Determination and Use of Response Densities. *J. Mol. Struct. THEOCHEM* **1991**,*80*, 95-126.

- [53] Gauss, J.; Cremer, D. Analytical Energy Gradients in Møller-Plesset Perturbation and Quadratic Configuration Interaction Methods: Theory and Application. *Adv. Quantum Chem.* **1992**, *23*, 205-299.
- [54] Carpenter, J. E.; Weinhold, F. Analysis of the Geometry of the Hydroxymethyl Radical by the "Different Hybrids for Different Spins" Natural Bond Orbital Procedure. *J. Mol. Struct. (Theochem)* **1988**, *46*, 41-62.
- [55] Reed, A. E.; Weinstock, R. B.; Weinhold, F. Natural Population Analysis. *J. Chem. Phys.* **1985**, *83*, 735-746.
- [56] Reed, A. E.; Curtiss, L. A.; Weinhold, F. Intermolecular Interactions from a Natural Bond Orbital, Donor-Acceptor Viewpoint. *Chem. Rev.* **1988**, *88*, 899-926.
- [57] Helgaker, T., Watson, M., Handy, N.C. Analytical Calculation of Nuclear Magnetic Resonance Indirect Spin-Spin Coupling Constants at the Generalized Gradient Approximation and Hybrid Levels of Density-Functional Theory. *J. Chem. Phys.* **2000**, *113*, 9402-9409.
- [58] Kutzelnigg, W.; Fleischer, U.; Schindler, M. in *NMR-Basic Principles and Progress*; Springer: Heidelberg, 1990, *23*, 165.
- [59] COLOGNE2000, Kraka, E.; Gräfenstein, J.; Gauss, J.; He, Y.; Reichel, F.; Olsson, L.; Konkoli, Z.; He, Z.; Cremer, D. Göteborg University, Göteborg, 2000.
- [60] Frisch, M. J.; Trucks, G. W.; Schlegel, H. B.; Scuseria, G. E.; Robb, M. A.; Cheeseman, J. R.; Zakrzewski, V. G.; Montgomery, Jr., J. A.; Stratmann, R. E.; Burant, J. C.; Dapprich, S.; Millam, J. M.; Daniels, A. D.; Kudin, K. N.; Strain, M. C.; Farkas, O.; Tomasi, J.; Barone, V.; Cossi, M.; Cammi, R.; Mennucci, B.; Pomelli, C.; Adamo, C.; Clifford, S.; Ochterski, J.; Petersson, G. A.; Ayala, P. Y.; Cui, Q.; Morokuma, K.; Malick, D. K.; Rabuck, A. D.; Raghavachari, K.; Foresman, J. B.; Cioslowski, J.; Ortiz, J. V.; Stefanov, B. B.; Liu, G.; Liashenko, A.; Piskorz, P.; Komaromi, I.; Gomperts, R.; Martin, R. L.; Fox, D. J.; Keith, T.; Al-Laham, M. A.; Peng, C. Y.; Nanayakkara, A.; Gonzalez, C.; Challacombe, M.; Gill, P. M. W.; Johnson, B.; Chen, W.; Wong, M. W.; Andres, J. L.; Gonzalez, C.; Head-Gordon, M.; Replogle, E. S.; Pople, J. A. *Gaussian 98, Revision A.5*, Gaussian, Inc., Pittsburgh PA, 1998.
- [61] Fantoni, R.; van Hlevoort, K.; Knippers, W.; Reuss, J. Direct Observation of Torsional Levels in Raman Spectra of Ethane. *Chem. Phys.* **1986**, *110*, 1-16.
- [62] Hirota, E.; Saito, S.; Endo, Y. Barrier to Internal Rotation in Ethane from the Microwave Spectrum of CH₃CHD₂. *J. Chem. Phys.*, **1979**, *71*, 1183-1187.
- [63] Munoz-Caro, C.; Nino, A.; Senent, M.L. Theoretical Study of the Effect of Torsional Anharmonicity on the Thermodynamic Properties of Methanol. *Chem. Phys. Lett.*, **1997**, *273*, 135-140.

- [64] For a recent review, see Goodman, L.; Pophristic, V. In *Encyclopedia of Computational Chemistry*, Schleyer, P.v.R.; Allinger, N.L.; Clark, T.; Gasteiger, J.; Kollman, P.A.; Schaefer III, H.F.; Schreiner, P.R. Eds. John Wiley:Chichester, UK, 1998, Vol. 4, p. 2525.
- [65] Kirby, A.J. *The Anomeric Effect and Related Stereoelectronic Effects at Oxygen*, Springer Verlag: New York, 1983.
- [66] Boykin, D.W. *¹⁷O NMR Spectroscopy in Organic Chemistry*, CRC Press, Boca Raton, 1991.
- [67] Perlin, A.S.; Casu, B. Carbon-13 and Proton Magnetic Resonance Spectra of D-glucose-13C. *Tetrahedron Lett.* **1969**, 2921-2924.
- [68] Podlasek, C.A.; Stripe, W.A.; Carmichael, I.; Shang, M.; Basu, B.; Serianmi, A.S. 13C-1H Spin-Coupling Constants in the β -D-Ribofuranosyl Ring: Effect of Ring Conformation on Coupling Magnitudes. *J. Am. Chem. Soc.* **1996**, *118*, 1413-1425.
- [69] Cavasotto, C.N.; Giribet, C.G.; Ruiz De Azua, M.C.; Contreras, R.H. Exo-Exo and Endo-Endo Vicinal Proton Spin-Spin Coupling Constants in Norbornane and Norbornene. An IPPP-CLOPPA Analysis. *J. Comput. Chem* **1991**, *12*, 141-146.
- [70] Barfield, M. in *Encyclopedia of Nuclear Magnetic Resonance*, Grant, D. M.; Harris, R. K., Edt.s, Wiley: Chichester, UK, 1996, p. 2520.
- [71] Marshall, J.; Walter, S. R.; Barfield, M.; Marchand, A. P.; Marchand, N. W.; Segre, A. L. Reasons for the Nonequivalence of the Exo-Exo and Endo-Endo Vicinal NMR Coupling Constants in Norbornanes. *Tetrahedron* **1976**, *32*, 537-542.